"High-resolution X-ray computed tomography in geosciences: a review of the current technology and applications"

V. Cnudde, M.N. Boone

PII: S0012-8252(13)00069-X
DOI: doi: 10.1016/j.earscirev.2013.04.003
Reference: EARTH 1847

To appear in: *Earth Science Reviews*

Received date: 1 June 2012
Accepted date: 12 April 2013

Please cite this article as: Cnudde, V., Boone, M.N., "High-resolution X-ray computed tomography in geosciences: a review of the current technology and applications", *Earth Science Reviews* (2013), doi: 10.1016/j.earscirev.2013.04.003

"High-resolution X-ray computed tomography in geosciences: a review of the current technology and applications"

Cnudde, V.[a], Boone, M.N.[b],

[a] *Dept. of Geology and Soil Science-UGCT, Ghent University, Krijgslaan 281 S8, B-9000, Ghent, Belgium*

[b] *Dept. of Physics and Astronomy-UGCT, Ghent University, Proeftuinstraat 86, B-9000 Ghent, Belgium*

Email address authors: veerle.cnudde@ugent.be; matthieu.boone@ugent.be;

Corresponding Author: Prof. Dr. Veerle Cnudde, veerle.cnudde@ugent.be; Department of Geology and Soil Science, Ghent University, Krijgslaan 281/S8, B-9000, Ghent, Belgium; Telephone: 0032 9 2644580; Fax: 0032 9 264 49 43

Abstract

High-resolution X-ray Computed Tomography (HRXCT) or micro-CT (µCT) is a frequently used non-destructive 3D imaging and analysis technique for the investigation of internal structures of a large variety of objects, including geomaterials. Although the possibilities of X-ray micro-CT are becoming better appreciated in earth science research, the demands on this technique are also approaching certain physical limitations. As such, there remains a lot of research to be done in order to solve all the technical problems that occur when higher demands are put on the technique. In this paper, a review of the principle, the advantages and limitations of X-ray CT itself are presented, together with an overview of some current applications of micro-CT in geosciences. One of the main advantages of this technique is the fact that it is a non-destructive characterization technique which allows 4D monitoring of internal structural changes at resolutions down to a few hundred nanometers. Limitations of this technique are the operator dependency for the 3D image analysis from the reconstructed data, the discretations effects and possible imaging artefacts. Driven by the technological and computational progress, the technique is continuously growing as an analysis tool in geosciences and is becoming one of the standard techniques, as is shown by the large and still increasing number of publications in this research area. It is foreseen that this number will continue to rise, and micro-CT will become an indispensable technique in the field of geosciences.

Keywords

High-resolution X-ray CT, geosciences, 3D analysis

Introduction

History and principle of X-ray CT

Since the discovery of a new type of radiation by Wilhelm Röntgen, *X-rays* have been used extensively in various research fields. A pertinent feature of this radiation type is its capability to penetrate material in varying degrees. This is mathematically formulated by Beer's law, which expresses the transmitted intensity I of a monochromatic X-ray passing an object:

$$I = I_0 e^{-\int \mu(s)\, ds} \quad (1)$$

where I_0 is the incident beam intensity and $\mu(s)$ is the local linear attenuation coefficient along the raypath s. The energy-dependent linear attenuation coefficient μ is determined by four effects, i.e. photoelectric effect, incoherent (Compton) scattering, coherent (Rayleigh) scattering and pair production. The latter can only occur at energies above 1.022 MeV and is thus not relevant in most X-ray CT setups. More information on this topic can be found in (Attix, 1986; Knoll, 2000).

This property was soon used for medical (Frost, 1896; Miller, 1896) and non-medical (Brühl, 1896) applications. In geosciences, the internal structure of a great diversity of geological samples has been examined by radiographic imaging mainly in the last 50 years (Baker and Friedman, 1969; Bjerreskov, 1978; Bouma, 1964; Calvert and Veevers, 1962; Hamblin, 1962; Herm, 1973; Howard, 1968; Louis et al., 2007; Monna et al., 1997; Schmidt et al., 2007; Sturmer, 1973). Constant improvement of the equipment still makes it a very extensively used technique in a wide range of applications, of which the most known are medical radiography and security systems.

A major drawback of this technique is the loss of information in one dimension. Radiographs, which are sometimes called *projection* or *shadow* images, project a 3D object on a 2D detector plane, losing depth information. This can lead to misinterpretation of the images.

A new technique to overcome this disadvantage was developed in the 1970s called *Computerized transverse axial tomography* (Ambrose, 1976; Hounsfield, 1973; Ommaya *et al.*, 1976) (abbreviated *CAT* or *CT*). By acquiring projection images from different directions, a 3D volume is reconstructed using dedicated computer algorithms. This 3D reconstruction technique was almost immediately used for medical applications, allowing visualisation of the human body and brain (Gawler *et al.*, 1974; Ledley *et al.*, 1974; Paxton and Ambrose, 1974). Applications in other research domains such as wood technology (Onoe et al., 1983; Taylor et al., 1984), palaeontology (Conroy and Vannier, 1987; Zollikofer et al., 1998), soil science (Anderson et al., 1988; Braz et al., 2000; Crestana et al., 1986; Crestana et al., 1985; Petrovic et al., 1982), marine sciences (Boespflug et al., 1995) and geosciences in general (Coles et al., 1991; Vinegar and Wellington, 1987; Wellington and Vinegar, 1987), as well as industrial applications (Hopkins et al., 1981) followed shortly.

From equation (1), it can be understood that the integrated linear attenuation coefficient can be easily derived at each point of a radiograph:

$$\int \mu(s)ds = -\ln\left(\frac{I}{I_0}\right) \quad (2)$$

By application of a rotational movement of the sample relative to the X-ray source and detector system, a number of different angular *projection images* are made. By using appropriate reconstruction algorithms (Herman, 1980; Herman and Natterer, 1981; Kak and Slaney, 1988), the local value of μ can be calculated for each point inside the scanned volume. The value of μ depends on the material density ρ and the mass attenuation coefficient μ/ρ, which is a tabulated and energy-dependent value and is approximately proportional to Z^3 in the X-ray energy range typically used for CT, with Z the atomic number (Attix, 1986; Knoll, 2000). Knowledge of this value thus does not allow a unique identification of the material or its density, unless one of them is known in advance.

It must be noted that this is only valid for monochromatic X-rays which follow a straight path. It will be demonstrated in following sections that these assumptions are not met, resulting in reconstruction artefacts.

X-ray CT has become more commonplace in the earth sciences for imaging geological samples at ambient conditions (Ketcham and Carlson, 2001; Lesher et al., 2009; Rivers et al., 2004). Medical CT and industrial CT systems, with typical spatial resolutions of 250 µm voxel size, are often used for their large core scanning capabilities (Baraka-Lokmane *et al.*, 2009) and dual energy scanning possibilities for the chemical analysis of core samples (Purcell et al., 2009). When one is performing the study of core samples, the surface as well as the internal features, including bedding features, sedimentary structures, natural and coring-induced fractures, cement distribution, small-scale grain size variation and density variation can now be analysed (Coles et al., 1998; Coles et al., 1991; Orsi et al., 1994). Extensive research has included applications on the complex porosity and pore geometry of carbonate reservoirs (Purcell et al., 2009), rock-fluid analysis (Purcell et al., 2009; PyrakNolte et al., 1997; Wennberg et al., 2009), the performance of diverting agents in unconsolidated sandstones (Ribeiro et al., 2007a; Ribeiro et al., 2007b; Vinegar and Wellington, 1987; Wellington and Vinegar, 1987), the physical properties of permafrost layers (Calmels and Allard, 2008), gas hydrate dissociation (Denison et al., 1997; Okui et al., 2003), and many other topics in geosciences.

Although X-rays and gamma-rays are the most commonly used type of radiation in CT, the same principle can be applied to protons (Ito and Koyamaito, 1984; Takada *et al.*, 1988), neutrons (Baechler et al., 2002; Koeppe et al., 1981; Lehmann and Wagner, 2010; Overley, 1983) and heavy particles (Crowe et al., 1975; Ohno et al., 2004; Shinoda et al., 2006) as radiation source. These techniques are beyond the scope of this paper, and are therefore not discussed further.

Towards micro-CT

Over the years, medical CT scanners have been drastically improved in terms of image quality, imaging speed and deposited radiation dose. Following technological advances, different generations of CT scanners have been conceived (Goldman, 2007), with recent developments towards dual-energy (Flohr et al., 2006; Graser et al., 2009; Primak et al., 2007) and energy selective CT (Barber et al., 2011). Temporal resolution has improved to less than 100 ms (Flohr et al., 2009). In contrast, spatial resolution remains limited to several hundreds of micrometers due to the dimension of the investigated object, i.e. a human patient.

A new research field emerged in high-resolution X-ray tomography, commonly called *micro-CT*. This method was first discussed in the 1980's, using X-ray tubes (Elliott and Dover, 1982; Elliott and Dover, 1985; Sato et al., 1981), gamma-ray sources (Gilboy, 1984; Gilboy et al., 1982) and synchrotron radiation (Bonse et al., 1986; Flannery et al., 1987; Grodzins, 1983) as X-ray source. Due to their low brilliance, gamma-ray sources are rarely used in micro-CT, and throughout the years both synchrotron-based and lab-based (using X-ray tubes) micro-CT have developed rapidly. The high brilliance of synchrotron radiation results in a clear superiority in terms of achievable spatial resolution and signal-to-noise ratio (Baruchel et al., 2006), but the number of synchrotron facilities is limited and the operational cost is very high. Lab-based micro-CT systems (Jakubek et al., 2006; Masschaele et al., 2007) on the other hand have lower X-ray flux but are more cost-efficient. Nowadays, a large number of desktop CT systems exist (Sasov and Van Dyck, 1998) which are commercially available, making micro-CT accessible for a large number of researchers. Recent developments in terms of X-ray optics made lab-based micro-CT comparable to synchrotron-based micro-CT in terms of spatial resolution but at the drawback of a heavily reduced X-ray flux and thus increased measuring time.

Although there is no clear distinction between CT and micro-CT, only applications of the latter will be discussed in this article. The boundary between both techniques will be defined here at a spatial resolution of 200 µm, which is typically not achievable by medical CT devices. Sample sizes for micro-CT range from as large as 40 cm to as small as several micrometers, with typical sample sizes for micro-CT in geosciences ranging from 1 mm to 5 cm. Despite this difference, several of the limitations and advantages of X-ray micro-CT which will be discussed in following sections are also applicable to standard (medical) CT, although this will not always be mentioned explicitly.

Typical micro-CT setup

A large difference between conventional medical CT and micro-CT can be found in the rotational movement. In medical CT, the patient remains stationary, while the complete X-ray source and detector system rotates around the patient. In most micro-CT systems, it is the object under investigation that rotates, and X-ray source and detector remain stationary. This setup achieves a better mechanical stability which is required at high resolutions. An exception on the rotating sample are in-vivo small animal micro-CT scanners (Ritman, 2004; Schuster et al., 2004). These are usually designed for high-speed scanning at reduced

radiation dose, and are as such not optimized for geological applications. Nevertheless, their high scanning speed and stationary sample positioning can be useful for imaging dynamical processes in geological specimens.

The most common lab-based setup is the standard cone-beam micro-CT (Feldkamp et al., 1984; Turbell, 2001). In this setup, the conical X-ray beam makes geometrical magnification possible by positioning the object under investigation at any position between X-ray source and detector (Figure 1A). This way, the highest achievable resolution is mainly limited by the focal spot size of the X-ray source. A trade-off has to be made between low-flux transmission-type X-ray tubes which allow for a focal spot size below 1 µm, and high-flux reflection-type X-ray tubes where the focal spot is larger (Vlassenbroeck, 2009). More generally, a smaller focal spot size requires a reduced X-ray flux. This trade-off makes very high resolution micro-CT (<1 µm) difficult and time-consuming at lab-based setups. On the detector side, a range of technologies can be used due to the geometrical magnification. In most cases, a large a-Si flat-panel detector combined with a relatively thick scintillator screen is used to obtain a high dynamic range. Alternatively, X-ray optics can be used in combination with a high-flux source to achieve very high spatial resolution (Feser et al., 2008; Gelb et al., 2009).

At synchrotron sources, the X-ray beam is almost parallel, making geometrical magnification impossible without X-ray optics but has a high X-ray flux. This high flux can be detected by a thin scintillator screen, converting the X-rays to visible light (Figure 1B). This allows the use of optical magnification lenses to achieve high resolution (Koch et al., 1998). A trade-off exists between a very thin scintillator screen, increasing the obtained resolution but reducing the detection efficiency, or a thicker scintillator which increases the detection efficiency but reducing the highest achievable resolution (Stampanoni et al., 2002). Geometrical magnification can be achieved using Fresnel zone plates (Chao et al., 2005; Chu et al., 2008), resulting in very high resolution. Recently, ptychography has gained importance in the field of X-ray microscopy to achieve even smaller voxel size down to 10 nm (Dierolf et al., 2010; Godard et al., 2011; Schropp et al., 2012).

Advantages and limitations of X-ray micro-CT

In this section, some of the advantages and limitations of high-resolution X-ray CT with respect to other techniques are discussed. Although some of the limiting effects are intrinsic to the technique, several others are the subject of current research and are likely to have a reduced impact in the near future.

3D visualisation and analysis

The main advantage of (micro-)CT is the ability to perform three-dimensional imaging in a non-destructive way. It returns a 3D distribution of the local linear attenuation coefficient, which is often stored as a stack of virtual 2D slices for quick viewing. Specialized rendering

software such as Fiji, VGStudio or Avizo allow for visual inspection of this 3D volume based on this local linear attenuation coefficient.

Although this visual inspection is a great qualitative tool, quantitative results are often required. To obtain these quantitative results from the X-ray CT data, the complete 3D volume should be analysed in a dedicated software package. At the moment, several software packages are available, such as Avizo, VGStudio Max, MAVI, Blob3D (Ketcham, 2005), Pore3D (Brun et al., 2010), 3DMA-Rock (Lindquist, 2001), Morpho+ (Brabant et al., 2011; Vlassenbroeck et al., 2007) and Fiji (Schlindelin et al., 2012). Quantitative results from 3D analysis can include data on the overall texture of a material, component volume fractions, pore and grain size parameters and morphology (shape, sphericity, roundness,…), surface texture, and many more. Any kind of parameter can also be used for statistical analysis throughout the 3D volume.

In practice, this quantitative 3D analysis is often not straightforward and can be prone to several systematic errors caused by the effects described below. It is essential that micro-CT users are aware of the limitations and pitfalls while recording or analysing data.

Noise

Like all imaging techniques, X-ray imaging is subject to noise. The lower limit of this noise level is determined by the number of detected photons and equals Poisson noise. In practice, image noise is function of many parameters, particularly when a scintillator is used. For so-called photon counting detectors such as Medipix, this theoretical limit can be achieved due to the read-out electronics (Passmore et al., 2001; Tlustos et al., 2004).

Discretization effects

In practice, projection data is always acquired using a 1D or 2D pixelated detector. After reconstruction, a 3D matrix of volume elements (*voxels*) is obtained. This discretization has a large impact on the possibilities of high-resolution X-ray CT.

One of the main limitations of micro-CT (and CT in general) is the lowest achievable voxel size compared to the size of the object under investigation. Due to the rotational movement, the volume that is imaged is a cylinder with diameter

$$D = \frac{N_d p_d}{M} \cos \alpha \qquad (4)$$

where N_d is the number of detector pixels, p_d the distance between the center of two neighbouring pixels, M the geometrical magnification defined as the ratio of the source-to-detector distance over the source-to-object distance and α the cone angle of the X-ray beam (Vlassenbroeck, 2009). In case of parallel-beam micro-CT, the latter two are equal to 1 and 0, respectively. Because this volume is divided into N_d pixels perpendicular to the rotational axis, the lowest achievable distance between the center of two neighbouring voxels (*reconstructed voxel size*) v_r is:

$$v_r = \frac{D}{N_d} = \frac{p_d}{M}\cos\alpha \quad (5)$$

To avoid severe imaging artefacts, this volume should have similar size as the complete sample (Kyrieleis et al., 2011). For technological and computational reasons, N_d is usually limited to several thousands of pixels, which sets a limit to the achievable voxel size as a function of the sample size.

All features which are smaller than this voxel size cannot be distinguished on the reconstructed dataset. Nevertheless, they do contribute to the reconstructed volume by means of the *partial volume effect*. The reconstructed value in each voxel is the average value of μ over the complete volume of that voxel. This also affects voxels which include an interface between structures, giving these voxels an intermediate grey value. This can be beneficial for visualisation and conversion to computer models for monomaterials (Young et al., 2008), but it is generally an imaging arefact reducing the accuracy of the data analysis (Ketcham and Carlson, 2001). More specifically this effect may result in a large error when analysing small structures and pores with a large ratio of surface to volume (Kerckhofs et al., 2008).

It is worth mentioning that voxel size is often confused with spatial resolution. The latter is a measure for the resolving power of an imaging system based on the modulation transfer function (MTF) of the complete imaging system, expressed in line pairs per distance unit. Due to the complexity of the MTF, the term resolution is commonly used to denote the reconstructed voxel size. It must be noted that the term resolution can also denote the number of pixels or voxels in an image.

Non-destructive technique

One of the main advantages of (micro-)CT is the non-destructive nature of the technique. It allows one to investigate the interior of an object without sacrificing it. This is a very valuable property, as it permits investigation of unique or valuable objects (Murphy et al., 2003), investigation of live objects, investigation of structural changes in one and the same sample under influence of environmental changes (Rozenbaum, 2011; Van den Bulcke et al., 2009) or mechanical stress (Saadatfar et al., 2012; Zabler et al., 2008), high-speed time-lapse monitoring (Mokso et al., 2011) etc. The monitoring of structural dynamic processes by means of X-ray CT is a big advantage since samples can be monitored and analysed in 3D under changing conditions, allowing to really visualise processes at a pore-scale level. Nevertheless, several conditions limit this advantage.

As mentioned before, the achievable voxel size is limited by the sample size. This makes it often necessary to take small sub-samples. The representativeness of the sample may be limited by this operation, making a well-considered compromise between voxel size and representative sample size necessary (Gy, 1976). Taking sub-samples might also influence the behaviour of the sample, e.g. under influence of mechanical stress or vibrations caused by drilling. Additionally, physical properties and behaviour, both intended and unintended, will mostly change when the dimensions of the object are altered. After taking the subsample, the original sample is modified, which can be undesirable in some cases. Several methods exist

to extend the reconstructed area (Pfeiffer, 2004; Zamyatin et al., 2005), to reconstruct horizontally truncated data (Defrise et al., 2006; Vlassenbroeck, 2009) or to overcome the limitation by mosaic scanning (Haberthür et al., 2010; Mokso et al., 2012), but the link between sample size and voxel size remains. Particularly in geosciences, where heterogeneity is an important characteristic, multi-scale imaging is gaining importance. In this technique, high resolution scans of small subsamples are used for characterization and modelling, and are spatially registered with low resolution scans of a large sample, providing macroscopic information (Grader et al., 2009).

Another effect that has to be considered in this context is sample positioning and sample stability. Tomographic reconstruction requires a rigid sample which does not move during the CT scan. In some cases, particularly when going to very high spatial resolution, special care is needed to achieve this, e.g. by consolidation or fixation of the sample. This can be considered as destruction of the original sample.

Operator dependency

Due to the variety in sample size, shape and composition, no fixed and generally accepted protocols exist for micro-CT scanning. This means a large amount of free parameters can be chosen arbitrarily, such as tube voltage, beam filtering, total exposure time, etc., all influencing the final result. Additionally, different micro-CT setups will yield different results, and the absence of generally accepted calibration phantoms, particularly in non-biomedical applications, hinders reliable comparison of results obtained at different setups.

Besides the operator-dependent image acquisition, obtaining quantitative results from the 3D volume is crucial. Therefore, the volume needs to be analysed using 3D analysis software. The most critical operation in this analysis is the segmentation of the volume, which is usually based on grey value thresholding. Due to effects such as partial volume and image noise, this step is extremely operator dependant (Baveye et al., 2010). Nevertheless, when analysing reconstructed volumes of similar objects, this error is a constant making comparison of these similar objects possible. The quantitative results obtained by 3D analysis can thus be considered as relative rather than absolute numbers. In recent years, other segmentation algorithms dealing with this issue have gained importance (Iassonov et al., 2009).

Imaging artefacts

As mentioned before, equation (3) is only valid in the case of monochromatic radiation. This condition can be met for synchrotron radiation, which can achieve a relative bandwidth of the order of 10^{-4} (Stampanoni et al., 2006). For laboratory-based setups, this condition is not met due to the Brehmsstrahlung-spectrum. This polychromaticity gives rise to one of the main imaging artefacts in X-ray CT, i.e. beam hardening. This effect is caused by the energy dependence of the linear attenuation coefficient μ, which implies low-energetic (*soft*) X-rays to have a higher probability of being absorbed than high-energetic (*hard*) X-rays. The result is an increase in reconstructed attenuation coefficient at the outer regions of the sample, i.e. the so-called *cupping effect*, referring to the shape of a cross-sectional line profile. The

cupping effect can be diminished by using beam hardening filters, which eliminate the soft X-rays, but a trade-off between X-ray flux and beam hardening arises. Also, several software corrections exist to deal with the beam-hardening effect (e.g. (Van de Casteele et al., 2002)). These correction methods attain good results for most samples, but may fail for complex samples with a variety of different materials.

A second artefact arises from the conical beam in common lab-based CT. Due to the incomplete sampling of the 3D Radon space (Kak and Slaney, 1988; Turbell, 2001), slices which are far away from the center of the cone can suffer severe artefacts from the so-called *cone-beam effect*. This is often a problem when investigating layered structures and surfaces of samples. This effect is diminished by using iterative reconstruction methods, and is completely removed by using a helical scanning trajectory (De Witte, 2010).

A third major artefact arises from the temporal or spatial coherence of the X-ray beam, and is called *phase contrast*. It can be approximated as the refraction of the X-rays, and is visualised as an edge-enhancement effect (Wilkins et al., 1984). This effect can be favourable for visual contrast (Tafforeau et al., 2006), but it often hinders correct segmentation and image analysis when left unprocessed. At laboratory-based setups, this effect mainly arises at very high resolution and low sample attenuation. Due to the high coherence of synchrotron radiation, the phase contrast effect is much more pronounced in a wide range of applications. Several imaging and processing methods are available to benefit from this effect or to correct for the phase artefacts (Boone et al., 2012a; Cloetens et al., 1999; David et al., 2007; Weitkamp et al., 2011).

Besides these major artefacts, caused by the imaging physics or the reconstruction mathematics, other imaging artefacts can occur. Common examples of these are ring artefacts, caused by the failure of one or more pixels in a pixellated detector or by the non-linearity of different pixels (Sijbers and Postnov, 2004), streak artefacts, usually caused by highly-attenuating inclusions (De Man et al., 1998), and artefacts caused by instability or movement of the sample. Less common artefacts include secondary radiation effects (Boone et al., 2012b), detector lag (Siewerdsen and Jaffray, 1999) and charge sharing effects (Firsching, 2009).

Data fusion:

The output of micro-CT scanning is a reconstructed 3D volume of local X-ray attenuation coefficients, which depend on both material composition and density. Although this is often sufficient, e.g. when the main interest is the morphology of the sample under investigation, sometimes more information is required, e.g. mineralogical information. This additional information requires other imaging techniques, which are usually not capable of imaging a 3D volume. For this reason, merging 3D CT data with 2D (Sakellariou et al., 2010; Sok et al., 2010) or 3D (Bruyndonckx et al., 2011) data from other techniques has become a key operation.

Besides data fusion from different techniques, multiple micro-CT datasets can also be fused to obtain multi-scale imaging or time-lapse imaging and analysis. In the first case, datasets at

different voxel sizes are combined to analyse larger volumes at high resolution(Grader et al., 2009). The latter case can be split up in two sub-categories. The first is rigid alignment, where the matrix is a rigid body that has been scanned several times. Between two scans, the sample has often been removed from the scanner, creating the need for alignment (Dewanckele et al., 2012). The second subcategory is non-rigid deformation, where a sample has deformed and deformation needs to be quantified (Ando et al., 2012; Hall et al., 2010).

Recently, much work has been done to improve this data fusion. In some cases, dataset fusion is performed completely manually (Boone et al., 2011), which is often a time-consuming and operator-dependent analysis step that is prone to biasing. In other cases, semi-automatic data fusion is used (Lenoir et al., 2007). However, inherent to these methods is the fact that they are often less flexible.

X-ray micro-CT used in geosciences:

In the following, a brief and limited overview of applications of micro-CT in geosciences is given, categorized in specific disciplines. It must be emphasized that many other references exist, and that this overview is merely an indication of the wide range of possibilities of micro-CT.

- 3D pore characterization

Before X-ray micro-CT became available, 3D pore characterization was only possible through statistical models for reconstructing 3D porous media from 2D thin section images (Hazlett, 1997) or by process-based models (Øren and Bakke, 2002). Both statistical and process based models have their advantages, but due to the current evolution in X-ray technology, complex pore-networks in 3D down to sub-micron scale can be imaged (Brunke et al., 2007; Brunke et al., 2010; Sakellariou et al., 2010; Sok et al., 2010; Weinekoetter, 2008).

Whilst previous pore characterization mostly relied on subjective 2D descriptions of 3D pore structures (Vazquez-Calvo et al., 2007) or by means of computerized reconstructed models (Latief et al., 2010), recently, more and more X-ray CT is being used combined with image analysis to allow complex 3D characterization. Already in the early days of synchrotron X-ray micro-CT the technique was used to directly image the 3D pore structure of rocks at micrometers resolution. Coles et al. (1998) already tried to visualise fluid transport at a pore level using synchrotron X-ray micro-CT, while Coles et al. (1998; 1994) and Spanne et al. (1994a; 1994b) studied not only soil-water-root processes but also topology and transport of porous media by synchrotron X-ray micro-CT.

McCoy et al. (2006) utilized micro-CT to unravel the origin of rare asteroidal vesicular basalts and to conduct numerical modelling of bubble formation in a dike of ascending magma. Modelling results indicate that thin (< 30 cm wide) dikes are trapped at approximately 5 km depth where about 75 ppm of CO and CO_2 contribute equally to vesicle formation. Vesicular eucrites were metamorphosed in this deep-seated environment, the gas was lost, and they were excavated by impacts. Polacci et al. (2010) similarly analysed the vesicular geometry in volcanic products to improve the understanding of volcanic processes.

Advances in non-destructive techniques such as micro-CT combined with spatial analysis, opened up the opportunity to directly quantify the internal architecture of soil in three dimensions (Sleutel et al., 2008) and the visualisation of soil organic matter (Bouckaert et al., 2009).

Porosity, pore-size distribution and pore geometry are some of the most important material properties for the investigation of weathering and conservation phenomena of natural building stones since they influence the permeability of water transport through the stone. By analysing the 3D pore structure and the internal dynamics of the stone by means of micro-CT, the potential weathering behaviour of a stone can be studied. Rozenbaum et al. (2011) investigated the general differences of a weathered and an unweathered sample of a similar stone. Alternatively, a sample can be artificially weathered and its structural changes can be visualised (Figure 2), e.g. in the case of a strong acid test (Dewanckele et al., 2012). Figure 2 represents the pore structure changes for a local building stone of Belgium (Lede stone, a calcareous sandstone) before weathering and after 10 days and 21 days of weathering using a strong acid test (Dewanckele et al., 2012). In the left column, the entire rendered volume is shown for the different steps, while in the right column only the 3D rendered pore structure is revealed. The red colour represents the largest pores (based on their volume) while the blue colour the smallest ones. In the first row (initial situation) the red pore structure corresponds to an elongated, dissolved shell fragment. Around this big pore, some smaller pores are visible. In contrast, on the second row (situation after 10 days of weathering) the red volume occupies less volume and new, relatively larger pores (in green) are formed on the edges of the sample. Finally, in the third row (situation after 21 days of weathering) the large shell fragment becomes connected with the newly formed pore structure on the border, resulting in one large interconnected pore structure (red structure). Some newly formed smaller pores (blue) are visible on the border of the sample.

Since in CT-technology, sample size is related to resolution, the production of drilled fixated stone samples with diameters down to 1 mm is crucial for high-resolution CT (Cnudde et al., 2009; Grader et al., 2009). Bhuiyan et al. (2013) analysed iron ore green pellets of approx. 12 mm in diameter by X-ray micro-CT. The segmented reconstructed volume represented a unique dataset consisting of a three-dimensional distribution of equiaxed objects corresponding to bubble cavities. This dataset was used to successfully validate a stereological method to determine the size distribution of spherical objects dispersed in a volume. This was achieved by investigating only a few cross-sectional images of this volume and measuring the profiles left by these objects in the cross-sectional images. Excellent agreement was observed between the size distribution of the bubble cavities obtained by directly classifying their size in the reconstructed volume and that estimated by applying the aforementioned stereological method to eight cross-sectional images of the reconstructed volume. Using different threshold values for binarization of the X-ray micro-CT data and comparing the results to those obtained by SEM, they found that X-ray micro-CT can be used after proper calibration against SEM data to measure the total porosity of the bubble cavities but can only provide a rough estimate of the median diameter because of the limited resolution achieved in this study.

- 3D grain analysis

Considerable progress has been made in 3D X-ray micro-CT as an imaging technique, resulting in a growing need for more flexible, complete analysis packages containing advanced algorithms in order to discriminate and quantify true distribution of mineral phases. Ikeda et al. (2004) performed an element-concentration mapping of a Cs-doped partially molten granite by means of synchrotron X-ray micro-CT. Jerram et al. (2009) studied 3D crystal size distributions of olivine in kimberlites, while Masad et al. (2005) computed particle surface characteristics. Similar analysis can be applied to any other porous material, e.g. specific mineral quantification in stone (Dewanckele et al., 2009) or the study of the variability in composition and texture of natural stones (Figure 3) in order to classify the material geologically and in order to assists in the understanding of the environmental conditions in which they are formed (Cnudde et al., 2012). Figure 3a represents a reconstructed 2D slice of a local Belgian sedimentary stone of the Ypresian (Eocene) which is a glauconite-bearing (5–10 %) arenite with silica cement scanned at a voxel size of 4.8^3 μm^3. Grains which are both rounded and very angular, with the occurrence of quartz splinters can be identified in the reconstructed slice. In Figure 3b, the glauconite grains (in different shades of green) can be separated from the quartz grains (orange to yellow), since there is enough contrast between both types of grains. Also a third mineral phase with an intermediate attenuation coefficient can be recognized (shown in grey on the coloured figure 3b), which is identified as feldspar using polarization microscopy. Based on stacks of 2D reconstructed slices, 3D image analysis makes it possible to digitally separate the different grains and determine for each grain the structural parameters like the volume, the surface, the sphericity, the maximum opening, the equivalent diameter and minimum closing. For the glauconite-bearing arenite three different minerals of the fieldstone were analyzed digitally: quartz, glauconite and feldspar. From coarse to fine, the different minerals are classified as medium sand to fine sand for the feldspar and quartz fraction and medium sand to very fine sand for the glauconite fraction. Quartz is very well sorted, feldspar well sorted and glauconite moderately sorted. The histogram of the glauconite shows a positive skew and represents a strongly fine-skewed distribution. However, quartz and feldspar are both coarse-skewed. The average sphericity for each grain size interval reveals a decrease in sphericity for smaller grain sizes for all different minerals. Benedix et al.(2008) conducted mineralogical and tomographic studies of previously unstudied millimetre- to centimetre-sized metal-sulphide-vesicle assemblages and chronologic studies of the silicate host. The surface textures of volcanic ash particles, which are important components of explosive eruptions, are the subject of intense research (Ersoy et al., 2010). The characterization of these ash surfaces is crucial for understanding the physics of volcanic plumes, remote sensing measurements of ash and aerosols, interfacial processes, modelling transportation and deposition of tephra and characterizing eruptive styles. Since micro-CT allows the measurements of the surface area and the volumes of individual ash particles, both this technique and SEM stereoscopic imaging are suggested by Ersoy et al. (2010) to be good candidate techniques for the characterization of textures on macro-pore regions of ash particles. Polacci et al. applied X-ray micro-CT to clasts of pumice and scoria from

Stromboli, Villarica and the Campanian ignimbrite (Polacci et al., 2006) and samples of scoria and pumice from normal and paroxysmal activity at Stromboli (Polacci et al., 2009). Gualda and Rivers (2006) presented crystal size distributions for pumice clasts from the Bishop Tuff (California). Since accessory minerals preserve important records of the evolution of magmatic systems, X-ray micro-CT was used to yield three-dimensional maps of selected elements, particularly zircon and rare earth elements, making it possible to qualitatively and quantitatively document the textures of these minerals *in situ* and in three dimensions (Gualda et al., 2010).

In the field of reservoir characterization, micro-CT has become an interesting research technique, not only for the quantification of the 3D heterogeneity of reservoir properties (Bera et al., 2010; Remeysen and Swennen, 2008) but also for the sedimentary and diagenetic phases (Grochau et al., 2010; Nakashima et al., 2008). Lesher et al. (2009) combined high-pressure set-ups and synchrotron radiation to model the Earth's thermal state, the chemical differentiation, and the dynamic processes, since it required knowledge of properties of silicate and metallic melts at high pressure. Sedimentary cores can be examined non-destructively in 3D as well as any kind of core. Pirlet et al. (2010; 2012) studied diagenetic formation of gypsum and dolomite and the mineral assemblages in cold-water coral mounds by means of micro-CT (Van Rooij et al., 2011). Arns et al. (2005a; 2005b) performed petrophysical analysis from reservoir core fragments and pore-scale characterization of carbonates by micro-CT. Uchida et al. (2000) examined the occurrences of natural gas hydrates beneath the permafrost in the Mackenzie Delta. Synchrotron experiments for studying core samples has previously been shown to provide excellent two- and three-dimensional high resolution descriptions of pore structure and mineral distributions of core material (Coenen et al., 2004; Coles et al., 1998).

Due to the increase in spatial and time resolution of X-ray micro-CT systems, it becomes possible to study particle deposition and particle dynamics. Imaging techniques like micro-CT can not only provide the morphological shape of internal particles, but also the sedimentary 3D structures that display a distinct density contrast with their surroundings (e.g. plant remains in lake sediments, sand dikes, etc.) (Carlson, 2006; Minter et al., 2012).

- Fracture analysis

For the study of fractures, representing mechanical failures of the rock strength to natural geological stresses such as tectonic movement, lithostatic pressure changes, thermal stresses, high fluid pressure, drilling activity, and even fluid withdrawal, highly advanced techniques like micro-CT can be used. Fluid flow interactions between fractures and the matrix have a significant impact on displacement processes. Alajmi and Grader (2009) focused on multiphase flow in the presence of a fracture tip. They studied two-phase fluid flow (water-oil) displacements in layered Berea sandstone that was artificially fractured with a single extensional fracture perpendicular to the natural layers. The temporal and spatial saturation distributions during the experiments of this study were determined using X-ray micro-CT. This 4D CT experimental data and recovery information were used as the basis for simulation

in an effort to determine the interaction of the fracture-matrix environment with multiphase flow. Bertels et al (2001) developed an experimental technique that uses X-ray micro-CT to provide high-resolution measurements of aperture distribution and *in situ* saturation along with capillary pressure and relative permeability for a rough-walled fracture.

Dvorkin et al. (2009), Karpyn et al. (2009) Petchsingto et al. (2009) Toumllke et al. (2010) and Kalam et al. (2011) all performed fluid flow modelling and digital rock physics on the digital micro-CT data. While Keller et al. (1999) studied the effect of fracture aperture variations on the dispersion of contaminants, Kellller (Keller, 1998) and Ketcham et al. (Ketcham et al., 2010) characterized fracture apertures by micro-CT (Figure 4). In Figure 4a, the reconstructed 2D slice after micro-CT scanning is shown, featuring a large pumice clast at a widening point of the fracture. The fracture aperture throughout the specimen is calculated and shown in Figure 4b. Zhu et al. (2007) studied tracer transport in fractured chalk by X-ray micro-CT and digital image-based simulation. Voltolini et al. (2011) investigated a mortar affected by alkali-silica reaction (ASR) and characterised the void space herein, identifying cracks from the ASR expansion.

Characterizing and understanding the porous media network structure and the fractures are essential for maintaining and enhancing oil and gas recovery, since the pore system controls the fluid transport processes, described by the permeability and diffusion. Studies of the vertical diffusion of tracer solution (sodium iodine, NaI) in a layered Berea Sandstone sample that was partially fractured by using X-ray CT for its monitoring and quantification allowed the correlation of the layers' porosity and diffusion rate (Alajmi et al., 2009).

- Multi-scale imaging

For both pore- and grain size analysis as well as any kind of 3D characterization by means of X-ray CT, there always is the link between the sample size and the obtained resolution. In order to overcome this problem, a range of experimental and computational tools have been developed which can assist one in probing the material’s structure across the wide range of scales in an integrated fashion (Wildenschild and Sheppard, 2012). Sok et al. (2010) and Grader et al. (2009) developed multi-scale imaging systems that uses thin sections from the original CT scanned sample or sub-samples, to image it at higher resolutions by means of X-ray CT, back-scattered and focussed ion beam scanning electron microscopy to deliver information of the grains and pores at submicron resolutions and combines this information with the data derived from the original CT dataset (Figure 5). In Figure 5a the schematic concept of the registration of a 2D SEM slice to a 3D micro-CT volume is given. In image registration, all the translation, rotation, warping and scaling transformations required to couple the SEM data to the slice of a 3D tomographic data set is undertaken (Sok et al., 2010). In Figure 5b the concept of mapping the image data from a high resolution 2D SEM to a slice of the tomogram is given. Generally, the resolution of tomographic is limited to ~1 µm while microscopy allows one to probe objects down to nanometer scale. Figure 5b illustrates the coupling of 250^2 nm² resolution SEM image to 2.85^3 µm³ micro-CT slice from a 3D data

set. Microporous features (e.g., porosity at submicron scales, pore size) from the higher resolution SEM can be mapped onto the corresponding slice of the tomogram. From this mapping features one can then stochastically propagate this higher resolution information throughout the 3D volumetric tomographic data.

- Ore analysis

Imaging techniques like micro-CT can provide unique information of the geological and metallurgical significance for gold and related ore minerals.
Kyle et al. (2008) examined the supergiant Grasberg porphyry Cu-Au deposit. Differentiating between metallic mineral grains with relatively small differences in density, e.g., bornite (5.1 g/cm3) from chalcopyrite (4.2 g/cm^3), is relatively straightforward for isolated monominerallic grains or composites in a similar lower-density matrix, but difficulties were encountered with the interpretation of typical intergrown ore minerals (Figure 6). X-ray beam-hardening artefacts could lead to inconsistency in attenuation determination, both within and among slice images, complicating quantitative processing. However, differentiation of chalcopyrite and bornite were successful in smaller-diameter (<= 22-mm) cores of Grasberg ores. Small-diameter (<= 10 mm) cores of the Grasberg stockwork Cu-Au ore were analysed and data reduction protocols using the Blob3D program (Ketcham, 2005) were modified to improve the quantification of grain sizes and shapes. Grains as small as 6.5 µm were identified and all of these grains were in direct contact with chalcopyrite, providing support for gold distribution in porphyry copper systems being a result of exsolution from copper sulphides. Digital radiography combined with micro-CT scanning precisely defined the *in situ* location of mineral grains of interest within a sample, which then can be studied in conventional petrographic sections, and other types of analytical studies conducted, e.g., gold trace element geochemistry.

Ghorbani et al. (2011) used a micro-CT scanner for the 3-D characterization of crack and mineral dissemination in sphalerite ore particles. In order to distinguish between the different minerals, a dual energy scanning procedure was run to determine both the density and effective atomic number of the minerals of interest. Combination of this information with a prior knowledge of the mineralogical characteristics of the ore, allowed the differentiation of the major minerals of interest in 3-D (galena, sphalerite, pyrite and silicate gangue) without the need for laborious sample preparation (such as impregnating, thinning, polishing).
Ghorbani et al. (2011) reported the potential applications of X-ray CT to heap leaching technology and future directions. Agorhom et al (2012) mentions that there is a considerable challenge in accurate characterization of gold (Au) particles in low-grade plant ore mineral samples.

- Monitoring structural dynamic processes

The monitoring of structural dynamic processes requires some technical challenges when using X-ray CT. Preferably, process-oriented experiments are carried out in an X-ray CT system in such a way that no displacement of the sample is needed during different stages of the experiment, resulting in a sequence of 3D images that are perfectly aligned with one

another (Wildenschild and Sheppard, 2012). This perfect alignment is often crucial for further analysis. Unfortunately, in many occasions it is inconvenient to carry out all the experiments inside the X-ray CT systems due to the length of a certain kind of experiment. In these cases, alternating steps of imaging is needed as well as ex-situ sample modification (Wildenschild and Sheppard, 2012). Since it is impossible to position the samples during imaging with micron precision, alignment between the different imaging phases will be needed. Two methods exist to align these 3D data-sets after X-ray CT imaging: rigid body registration, when no deformation on the sample has occurred, and digital volume correlation, when the sample has been deformed during the experiment. Thanks to rigid body registration, a voxel-perfect alignment of all images will be obtained, however, this remains computationally difficult, especially when the images are also scaled differently (Wildenschild and Sheppard, 2012). In the case of sample deformation, Bay et al. (1999) generated a map showing the displacement vector of each voxel (i.e. a full strain map). The implementation of triaxial test cells in a micro-CT scanner (Charalampidou et al., 2011; Geraud et al., 1998; Hall et al., 2010; Lenoir et al., 2004; Otani et al., 2010; Raynaud et al., 2010; Siddiqui et al., 2010; Viggiani et al., 2004; Watanabe et al., 2009) can help to understand the stress- and time-dependent deformation of porous structures (Figure 7). The magnitude of the rotation of individual grains during triaxial compression tests, plotted for the vertical slices through the middle of the scanned specimen is shown in Figure 7a. In Figure 7b, the shear strain inside a scanned sample during similar experiment is plotted. The combination of micro-CT scanning and the use of a triaxial test cells helps to predict changes in reservoir production, by analysing the behaviour of the most important properties of the rock, such as porosity and permeability (Charalampidou et al., 2011; Karacan and Mitchell, 2003).

Temperature-controlled imaging can be very important for many research topics, including those where probe flow and transport systems are related to the deeper subsurface environment like oil recovery processes, geothermal energy recovery, and geological sequestration of CO_2 (Wildenschild and Sheppard, 2012). Micro-CT was used to represent models of the internal composition and structure of undisturbed pro- and subglacial soft sediment sample plugs for the purposes of identifying and analysing kinematic indicators (Tarplee et al., 2011). Since 2001, research on snow by means of a cryo-stat is being performed. Coleou et al. (2001) and Heggli et al. (2011) imaged and measured snow in 3D, while Flin et al. (2004) characterized the snow microstructural evolution under isothermal conditions. Kaempfer et al. (2005) described a microstructural approach to model heat transfer in snow, while Pieritz et al. (2004) modelled the micromechanics of snow. Schneebeli and Sokratov (2004) performed tomography of the temperature gradient metamorphism of snow and associated changes in heat conductivity.

Some of the technical difficulties, when visualising pore-scale resolving processes are the required small sample size and thus weakness of such thin samples as well as the need to obtain sufficient contrast between the pore fluids inside the material and the related difficulties to threshold these correctly (Silin et al., 2011). In 2011, Iglauer et al. (2011)were able to image residual CO_2 in sandstone by means of X-ray CT at temperature and pressure corresponding to CO_2 in its supercritical state.

In soil science, deformation is a perpetual process in the pedosphere where besides physicochemical stresses primarily alternating hydraulic and mechanical stresses continuously re-arrange the configuration of solid particles. Peth (2010) and Peth et al. (2010) studied local strain and changes in soil structure resulting from hydraulic and mechanical stresses based on X-ray micro-CT data. Digital image reconstructions were used to quantify local structural pore space characteristics and local soil deformation by 3D morphological and correlation analysis of grayscale tomograms. The results demonstrate the potential of more detailed non-invasive micro-mechanical analysis of soil deformation processes which could improve the conceptual understanding of the physical behaviour of soil systems.

Analogue models, commonly used to gain insights into large-scale volcano-tectonic processes, were scanned by means of micro-CT, documenting model surface topography and the three-dimensional (3D) aspect of deformation structures in order to understand the simulated processes (Kervyn et al., 2010). This method allows documenting the deformation of the brittle-ductile interface and turns out to be a powerful tool for better understanding the complex 3D deformation associated with volcano-tectonic processes.

- Fluid flow analysis

Currently it is possible to fit various pieces of equipment interconnected with fluid flow lines in the working space of different X-ray CT systems. The only constrains for fluid flow experiments is that, in order to get high quality images, the internal processes should be much slower than or stable during the scanning time. Additionally, enough exposure time is needed in order to obtain a good signal-to-noise ratio, meaning that there will always be a trade-off between acquisition time and image quality. However, it remains a challenge to perform process-oriented experiments that are carried out at a X-ray CT scanner due to the constrains of the sizes of the working space and by the ability to run fluid flow lines to and from the fluid flow cell, since additionally, there is the need, in many cases, for the attached fluid lines to be able to rotate (180° up until 360°) with the sample as it rotates in the beam (Wildenschild and Sheppard, 2012).
Using calculations derived from fluid flow modelling, based on 3D images from techniques like micro-CT (Petchsingto and Karpyn, 2009), predictions on diffusion of contaminants can be estimated (Polak et al., 2003). Based on these calculations, suggestions on possible remediation efforts like clean water injection into the fractures can be tested. To be able to predict contaminant transport in groundwater, an accurate conceptual and physical understanding of aquifer properties at multiple scales is required. Dann et al. (2011) derive the physical and hydraulic properties of a coastal sand aquifer using micro and macro X-ray computed tomography techniques. Singh et al. (2011) examined the pore-scale behavior of a non-aqueous phase liquid (NAPL) trapped as residual contamination in a porous medium, subject to freeze-thaw cycles, by X-ray micro-CT (Figure 8). By means of X-ray CT it was possible the render in 3D an X-ray tomogram of residual non-aqueous phase liquid (yellow) and water (blue) in bead pack (transparent). Ketcham and Iturrinno (2005) developed a

method that allowed them to study fluid penetration into volcanic rocks. Chen et al. (2009) used X-ray micro-CT and pore scale modelling to quantify sediment mixing and fluid flow in a developing streambed.

Natural building stones are heterogeneous substances characterized by a wide range of mineral compositions, textures and structures. Consequently, their physical and chemical properties and the resulting durability are quite variable. When studying natural building stones, it is of prime importance to address their characteristic properties. For many years, most characterization and flow and transport experiments were carried out first in the laboratory and before and/or afterwards X-ray imaging was done for evaluation. Since it has become more feasible to perform a selective range of experiments directly on the X-ray CT scanner, such that disturbance from transportation can be avoided and registration issues are simplified (Wildenschild & Sheppard) many fluid flow experiments are being performed directly an a X-ray CT scanner to monitor the dynamics. Fluid-flow in building stones (Cnudde et al., 2008; Coles et al., 1998; Wennberg et al., 2009; Xin et al., 2010) can be studied by means of X-ray CT (Cnudde et al., 2011) together with their weathering resistance (Navarre-Sitchler et al., 2009) against frost-thaw (Ingham, 2005), thermal shock (Török and Prikryl, 2010), salt (Charola, 2000), etc. Based on these studies one can provide advice on the application of building stones and their use as restoration product (Hanley and Pavía, 2008; Lanas et al., 2004; Maravelaki-Kalaitzaki et al., 2005; Rizzo and Megna, 2008; Szemerey-Kiss and Török, 2011).
Tight gas reservoirs exhibit storage and flow characteristics which are intimately tied to depositional and diagenetic processes (Golab et al., 2010). As a result, exploitation of these resources requires comprehensive reservoir description and characterization programs to identify properties which control production. In particular, tight gas reservoirs have significant primary and secondary porosity and pore connectivity dominated by clays and slot-like pores, which makes them particularly susceptible to the effects of overburden stress and variable water saturation. Golab et al. (2010) studied those tight gas reservoirs by means of X-ray CT.

In petroleum reservoir engineering, a realistic characterization of heterogenic reservoir rocks has been a long-standing problem of great practical interest because it may significantly affect the productivity of these reservoir systems (Qi et al., 2000; Santos et al., 2002). Integrated application of combined micro-CT characterization and process monitoring, with modelling could demonstrate the importance of rock heterogeneity (porosity, hydraulic conductivity, and diffusivity) in fluid transport processes (Kumar et al., 2010a; Kumar et al., 2010b; Watanabe et al., 2011a; Watanabe et al., 2011b). The petrophysical features of reservoir rocks can therefore be studied not only in the context of fluid flow but also as means of evaluating reservoir quality (Carlson, 2006).

Combined with fluid flow visualisation, electronical and acoustic measurements can also be performed during X-ray imaging, for example the experiments of Redwan & Rammlmeir (2010) who simultaneously measured the electronical conductivity and water saturation

through X-ray imaging using an experimental setup involving the use of a geophysical foil that allowed them to monitor changes in electrical conductivity.

- Morphological characterization of fossils

Due to the non-destructive-nature of X-ray micro-CT, rare and valuable artefacts can be examined in 3D. Donoghue et al. (2006) investigate fossilized embryos, whereas Tafforeau et al.(2006) cover a wide range of fossils. More recently, Gai et al. (2011) characterized a fossil of a jawless fish using synchrotron-based micro-CT. Other types of fossils include animals which have been preserved in amber (Dierick et al., 2007), such as spiders (Bosselaers et al., 2010; Penney et al., 2007), beetles (Perreau and Tafforeau, 2011), pseudoscorpions (Figure 9, which shows in high detail the right chelal fingers of the *Pseudogarypus synchrotron* Henderickx et al, 2012 at a reconstructed voxel size of 0.667^3 μm^3) (Henderickx et al., 2006; Henderickx et al., 2012) and earwigs (Perrichot et al., 2011). Other than these natural artefacts, man-made prehistoric objects are the subject of the research of Abel et al. (2011).
At sub-micron resolutions, three-dimensional imaging and bio-metric quantification of fossils like foraminiferal interiors becomes possible. Thanks to this technique a new era can be opened in fundamental biometric-evolutionary research; it can provide a means of morphologic evaluation of phylogenies based on molecular data. Eventually, the accuracy of palaeoceanographic and palaeoclimatic reconstructions could also benefit from the possibility of morphological differentiation between cryptic planktonic species (Speijer et al., 2008).

Conclusion

Although the possibilities of X-ray micro-CT are increasingly well-known and used in almost all research fields in earth sciences, several challenges remain to be tackled. Despite technological and computational advances, discretization effects and the consequences thereof, such as the partial volume effect and the relation between sample size and voxel size, are issues that are to be kept in mind when performing X-ray CT analysis. Like in many other microscopical techniques, working at high resolutions on small objects requires proper knowledge of the limitations and optimization of the workflow, especially when working with heterogeneous materials. At the same time, 3D analysis of large digital volumes has become possible: image segmentation has improved, the computation power has increased, new and better performing algorithms were developed and new characterization parameters are established. Some physical limitations, such as X-ray spot sizes are in some cases reached, indicating the technique has reached a mature state.

Nevertheless, knowledge in geosciences is often still missing 3D visualisations of structural details or the monitoring of dynamic processes at high resolutions. Technically high resolution X-ray CT has a lot to offer for geosciences and it is up to the researchers to explore

the new applications which can benefit from the possibilities of this technique. Like any other technique, it is important to know its limitations and use it in the most optimal way. The fact that high resolution X-ray CT is a non-destructive technique is extremely important for the geomaterial research: it allows fusing obtained 3D data with chemical or structural data obtained from other techniques, to visualise and analyse dynamic processes and thus provide better insights in the structure, internal processes and many more.

Additionally, new technologies are breaking through, which have the potential to greatly improve the possibilities of X-ray micro-CT. Techniques that make use of the energy-dependence of the attenuation coefficient, such as dual-energy CT and spectral CT, are being explored to improve material identification, one of the main issues in micro-CT. The combination of micro-CT with complementary techniques takes advantage of increased computational possibilities for image correlation and advances in the field of these techniques, which often explore 2D, pseudo-3D or even full 3D spatial information. Increasing computational power mainly improves analysis possibilities, in the first place by accelerating 3D analysis algorithms and making new analysis algorithms feasible, but also by enabling modelling to extend quantitative results beyond the scanned sample. Besides all these technological advances with increasing use of micro-CT in geosciences, the standardization will naturally be established, yielding more reliable results, comparable to medical CT scanning.

Acknowledgements

The authors acknowledge the entire UGCT team for the fruitful discussions on all aspects of micro-CT. Prof. Neil Davies, Prof. Luc Van Hoorebeke and Dr. Manuel Dierick are gratefully acknowledged for their review of the manuscript. J. Dewanckele, R. Ketcham, A. Alajmi, R. Sok, J. Kyle, E. Charalampidou, K. Singh, and H. Henderickx are acknowledged for providing the original figures for reprint.

Figure captions

Figure 1A: Schematic diagram of a typical lab-based micro-CT setup with a conical X-ray beam which allows geometrical magnification.

Figure 1B: Schematic diagram of a typical synchrotron-based micro-CT setup. A white (polychromatic) X-ray beam is created in the synchrotron by means of a bending magnet,wiggler or undulator. After a long propagation distance, this beam passes the monochromator, selecting an energy with a certain bandwidth (quasi-monochromatic or pink beam). This quasi-parallel pink beam is attenuated by the sample and converted to visible light by means of a scintillator screen. Subsequently, optics are used to magnify this image onto a visible light detector.

Figure 2: 3D rendered volumes of a calcareous sandstone (left column) and the pore volume colour-coded by their equivalent diameter (ED) (right column): in red: the largest pores (based on their equivalent diameter) while the blue colour the smallest ones. The sample is artificially weathered by means of a strong acid test during 21 days and scanned before (top row), during (middle row) and after (bottom row) this process. Reprinted from (Dewanckele et al., 2012), Copyright (2012), with permission from Elsevier.

Figure 3: (a) Reconstructed slice of a glauconite-bearing arenite; (b) corresponding slice where the grains are colour-coded based on the maximum opening of the grain after digital image analysis. The glauconite grains (represented in shades of green; with small (darker) to bigger (lighter) maximum opening) can be separated from the quartz grains (yellow to red objects represent with small (yellow) to larger (red) maximum opening), since there is enough contrast between both types of grains. Also a third mineral phase with an intermediate attenuation coefficient can be recognized (shown in grey on the coloured figure), which is identified as feldspar using polarization microscopy. Reprinted from (Cnudde et al., 2012), Copyright (2012), with permission from the Mineralogical Association of Canada.

Figure 4: Results of CT scanning and measurement of a fracture in a welded tuff sample; (a) a typical slice, featuring a large pumice clast at a widening point of the fracture; (b) a two-dimensional map of the fracture aperture throughout the specimen. Altered figure from (Ketcham et al., 2010), with permission.

Figure 5: (a) Schematic of 2D SEM to 3D micro-CT registration; (b) Example of the mapping of microporosity from a registered slice of a micro-CT dataset (upper region) to the higher resolution in the SEM image (lower region). Reprinted from (Sok et al., 2010), Copyright (2010), with permission from SPWLA.

Figure 6: Representative slices of a Main Grasberg intrusion breccia core showing differentiation of magnetite (mt), chalcopyrite (cp), bornite (bn) and gold (Au) in a potassically altered groundmass. Altered figure from (Kyle et al., 2008), with permission.

Figure 7: a) Magnitude of the rotation of individual grains during triaxial compression test, plotted for the vertical slices through the middle of the specimen. Altered figure from (Hall et al., 2010), with permission; b) Shear strain inside the sample during similar experiments. Altered figure from (Charalampidou et al., 2011), with permission.

Figure 8: Rendered X-ray tomogram of residual non-aqueous phase liquid (yellow) and water (blue) in bead pack (transparent). Reprinted with permission from (Singh et al., 2011); Copyright (2011) American Chemical Society.

Figure 9: A high resolution detail (reconstructed voxel size 0.667^3 μm^3) of the right chelal fingers of a *Pseudogarypus synchrotron* Henderickx et al, 2012 fossil trapped in amber imaged using propagation-based phase contrast synchrotron micro-CT. Altered figure from (Henderickx et al., 2012) with permission.

References

Abel, R.L., Parfitt, S., Ashton, N., Lewis, S.G., Scott, B. and Stringer, C., 2011. Digital preservation and dissemination of ancient lithic technology with modern micro-CT. Computers & Graphics, 35(4): 878-884.

Agorhom, E.A., Skinner, W. and Zanin, M., 2012. Upgrading of low-grade gold ore samples for improved particle characterisation using Micro-CT and SEM/EDX. Advanced Powder Technology, 23(4): 498-508.

Alajmi, A.F. and Grader, A., 2009. Influence of Fracture Tip on Fluid Flow Displacements. Journal of Porous Media, 12(5): 435-447.

Alajmi, A.F., Grader, A. and Alkafeef, S.F., 2009. Evaluation of Tracer Diffusion in Layered System Using X-Ray CT. Petroleum Science and Technology, 27(11): 1134-1150.

Ambrose, J., 1976. Computerized transverse axial scanning (tomography): Part II. Clinical application. British Journal of Radiology, 46(552): 1023-1047.

Anderson, S.H., Gantzer, C.J., Boone, J.M. and Tully, R.J., 1988. Rapid nondestructive bulk-density and soil-water content determination by computed-tomography. Soil Science Society of America Journal, 52(1): 35-40.

Ando, E., Hall, S.A., viggiani, G., Desrues, J. and Besuelle, P., 2012. Grain-scale experimental investigation of localised deformation in sand: a discrete particle tracking approach. Acta Geotechnica, 7(1): 1-13.

Arns, C.H., Bauget, F., Ghous, A., SakellarioU, A., Senden, T.J., Sheppard, A.P., Sok, R.M., Pinczewski, W.V., Kelly, J.C. and Knackstedt, M.A., 2005a. Digital core laboratory: Petrophysical analysis from 3D imaging of reservoir core fragments. Petrophysics, 46(4): 260-277.

Arns, C.H., Bauget, F., Limaye, A., Sakellariou, A., Senden, T.J., Sheppard, A.P., Sok, R.M., Pinczewski, W.V., Bakke, S., Berge, L.I., Oren, R.E. and Knackstedt, M.A., 2005b. Pore-scale characterization of carbonates using X-ray microtomography. Spe Journal, 10(4): 475-484.

Attix, F.H., 1986. Introduction to radiological physics and radiation dosimetry. Wiley-VCH.

Baechler, S., Masschaele, B., Cauwels, P., Dierick, M., Jolie, J., Materna, T. and Monderlaers, W., 2002. The new cold neutron tomography set-up at SINQ. Nuclear Instruments & Methods in Physics Research, Section A: Accelerators, Spectrometers, Detectors, and Associated Equipment, 481(1-3): 397-405.

Baker, S.R. and Friedman, G.M., 1969. A non-destructive core analysis technique using X-rays. Journal of Sedimentary Petrology, 39(4): 1371-1383.

Baraka-Lokmane, S., Main, I.G., Ngwenya, B.T. and Elphick, S.C., 2009. Application of complementary methods for more robust characterization of sandstone cores. Marine and Petroleum Geology, 26(1): 39-56.

Barber, W.C., Nygard, E., Wessel, J.C., Malakhov, N., Wawrzyniak, G., Hartsough, N.E., Gandhi, T. and Iwanczyk, J.S., 2011. Energy-resolved photon-counting x-ray imaging arrays for clinical K-edge CT, Nuclear Science Symposium and Medical Imaging Conference (NSS/MIC), Valencia, pp. 4441-4446.

Baruchel, J., Buffiere, J.-Y., Cloetens, P., Di Michiel, M., Ferrie, E., Ludwig, W., Maire, E. and Salvo, L., 2006. Advances in synchrotron radiation microtomography. Scripta Materialia, 55: 41-46.

Baveye, P.C., Laba, M., Otten, W., Bouckaert, L., Dello Sterpaio, P., Goswami, R.R., Grinev, D., Houston, A., Hu, Y., Liu, J., Mooney, S., Pajor, R., Sleutel, S., Tarquis, A., Wang, W., Wei, Q. and Sezgin, M., 2010. Observer-dependent variability of the thresholding step in the quantitative analysis of soil images and X-ray microtomography data. Geoderma, 157: 51-63.

Bay, B.K., Smith, T.S., Fyhrie, D.P. and Saad, M., 1999. Digital volume correlation: Three-dimensional strain mapping using X-ray tomography. Experimental Mechanics, 39(3): 217-226.

Benedix, G.K., Ketcham, R.A., Wilson, L., McCoy, T.J., Bogard, D.D., Garrison, D.H., Herzog, G.F., Xue, S., Klein, J. and Middleton, R., 2008. The formation and chronology of the PAT 91501 impact-melt L chondrite with vesicle-metal-sulfide assemblages. Geochimica Et Cosmochimica Acta, 72(9): 2417-2428.

Bera, B., Mitra, S.K. and Vick, D., 2010. Understanding the micro structure of Berea Sandstone by the simultaneous use of micro-computed tomography (micro-CT) and focused ion beam-scanning electron microscopy (FIB-SEM). Micron, 42(5): 412-418.

Bertels, S.P., DiCarlo, D.A. and Blunt, M.J., 2001. Measurement of aperture distribution, capillary pressure, relative permeability, and in situ saturation in a rock fracture using computed tomography scanning. Water Resources Research, 37(3): 649-662.

Bjerreskov, M., 1978. Discoveries on graptolites by X-ray studies. Acta Palaeontologica Polonica, 21(4): 463-471.

Boespflug, X., Long, B.F.N. and Occhietti, S., 1995. CAT-SCAN IN MARINE STRATIGRAPHY - A QUANTITATIVE APPROACH. Marine Geology, 122(4): 281-301.

Bonse, U., Johnson, Q., Nichols, M., Nusshardt, R., Krasnicki, S. and Kinney, J., 1986. High-resolution tomography with chemical specificity. Nuclear Instruments & Methods in Physics Research, Section A: Accelerators, Spectrometers, Detectors, and Associated Equipment, 246(1-3): 644-648.

Boone, M.N., De Witte, Y., Dierick, M., Almeida, A. and Van Hoorebeke, L., 2012a. Improved signal-to-noise ratio in laboratory-based phase contrast tomography. Microscopy and Microanalysis, 18(2): 399-405.

Boone, M.N., Dewanckele, J., Boone, M.A., Cnudde, V., Silversmit, G., Van Ranst, E., Jacobs, P., Vincze, L. and Van Hoorebeke, L., 2011. Three-dimensional phase separation and identification in granite. Geosphere, 7(1): 79-86.

Boone, M.N., Vlassenbroeck, J., Peetermans, S., Van Loo, D., Dierick, M. and Van Hoorebeke, L., 2012b. Secondary radiation in transmission-type X-ray tubes: simulation, practical issues and solution in the context of X-ray microtomography. Nuclear Instruments and Methods in Physics Research section A: Accelerators, Spectrometers, Detectors and Associated Equipment, 661(1): 7-12.

Bosselaers, J., Dierick, M., Cnudde, V., Masschaele, B., Van Hoorebeke, L. and Jacobs, P., 2010. High-resolution X-ray computed tomography of an extant new Donuea (Araneae: Liocranidae) species in Madagascan copal. Zootaxa(2427): 25-35.

Bouckaert, L., Van Loo, D., Sleutel, S., De Neve, S., Jacobs, P. and Van Hoorebeke, L., 2009. Application of X-ray tomography for quantification of the soil pore structure and visualization of soil organic matter. Geochimica Et Cosmochimica Acta, 73(13): A145-A145.

Bouma, A.H., 1964. Notes on X-ray interpretation of marine sediments. Marine Geology, 2: 278-309.

Brabant, L., Vlassenbroeck, J., De Witte, Y., Cnudde, V., Boone, M.N., Dewanckele, J. and Van Hoorebeke, L., 2011. Three-Dimensional Analysis of High-Resolution X-Ray Computed Tomography Data with Morpho+. Microscopy and Microanalysis, 17(2): 252-263.

Braz, D., Lopes, R.T. and Motta, L.M.G., 2000. Dual-energy computerized tomography in compacted soil. Geotechnical and Geological Engineering, 18: 221-238.

Brühl, 1896. Über Verwendung von Röntgenschen X-Strahlen zu paläontologisch-diagnostischen Zwecken. Achiv für Anatomie und Physiologie: 547-550.

Brun, F., Mancini, L., Kasae, P., Favretto, S., Dreossi, D. and Tromba, G., 2010. Pore3D: A software library for quantitative analysis of porous media. Nuclear Instruments & Methods in Physics Research, Section A: Accelerators, Spectrometers, Detectors, and Associated Equipment, 615: 326-332.

Brunke, O., Neuber, D. and Lehmann, D.K., 2007. NanoCT: visualizing of internal 3D-structures with submicrometer resolution, Materials Research Society Symposium: Materials, Processes, Integration and Reliability in Advanced Interconnects for Micro- and Nanoelectronics. Materials Research Society, San Francisco, CA,, pp. 325-331.

Brunke, O., Santillan, J. and Suppes, A., 2010. PRECISE 3D DIMENSIONAL METROLOGY USING HIGH RESOLUTION X-RAY COMPUTED TOMOGRAPHY (mu CT). In: S.R. Stock (Editor), Developments in X-Ray Tomography Vii. Proceedings of SPIE-The International Society for Optical Engineering. Spie-Int Soc Optical Engineering, Bellingham.

Bruyndonckx, P., Sasov, A. and Liu, X., 2011. Laboratory 3D Micro-XRF/Micro-CT Imaging System. In: I. McNulty, C. Eyberger and B. Lai (Editors), 10th International Conference on X-ray Microscopy. AIP Conference Proceedings, pp. 61-64.

Calmels, F. and Allard, M., 2008. Segregated ice structures in various heaved permafrost landforms through CT scan. Earth Surface Processes and Landforms, 33(2): 209-225.

Calvert, S.E. and Veevers, J.J., 1962. Minor structures of unconsolidated marine sediments revealed by X-ray radiography. Sedimentology, 1(4): 287-295.

Carlson, W., 2006. Three-dimensional imaging of earth and planetary materials. Earth and Planetary Science Letters 249: 133-147.

Chao, W., Harteneck, B.D., Liddle, J.A., Anderson, E.H. and Attwoord, D.T., 2005. Soft X-ray microscopy at a spatial resolution better than 15 nm. Nature, 435: 1210-1213.

Charalampidou, E.-M., Hall, S.A., Stanchits, S., Lewis, H. and Viggiani, G., 2011. Characterization of shear and compaction bands in a porous sandstone deformed under triaxial compression. Tectonophysics, 503(1-2): 8-17.

Charola, A.E., 2000. Salts in the deterioration of porous materials: An overview. Journal of the American Institute for Conservation, 39(3): 327-343.

Chen, C., Packman, A.I. and Gaillard, J.-F., 2009. Using X-ray micro-tomography and pore-scale modeling to quantify sediment mixing and fluid flow in a developing streambed. Geophysical Research Letters, 36: L08403.

Chu, Y.S., Yi, J.M., De Carlo, F., Shen, Q., Lee, W.-K., Wi, H.J., Wang, C.L., Wang, J.Y., Liu, C.J., Wang, C.H., Wu, S.R., Chien, C.C., Hwu, Y., Tkachuk, A., Yun, W., Feser, M., Liang, K.S., Yang, C.S., Je, J.H. and Margaritondo, G., 2008. Hard x-ray microscopy with Fresnel zone plates reaches 40 nm Rayleigh resolution. Applied Physics Letters, 92: 103119.

Cloetens, P., Ludwig, W., Baruchel, J., Van Dyck, D., Van Landuyts, J., Guigay, J.P. and Schlenker, M., 1999. Holotomography: Quantitative phase tomography with micrometer resolution using hard synchrotron radiation x rays. Applied Physics Letters, 75(19): 2912-2914.

Cnudde, V., Dewanckele, J., Boone, M., De Kock, T., Boone, M., Brabant, L., Dusar, M., de Ceukelaire, M., de Clercq, H., Hayen, R. and Jacobs, P., 2011. High-resolution X-ray CT for 3D petrography of ferruginous sandstone for an investigation of building stone decay. Microscopy Research and Technique, 74(11): 1006-1017.

Cnudde, V., Dewanckele, J., De Boever, W., Brabant, L. and De Kock, T., 2012. 3D characterization of grain size distributions in sandstone by means of X-ray computed tomography. In: P. Sylvester (Editor), Quantitative Mineralogy and Microanalysis of Sediments and Sedimentary Rocks. Mineralogical Association of Canada (MAC), pp. 99-113.

Cnudde, V., Dierick, M., Vlassenbroeck, J., Masschaele, B., Lehmann, E., Jacobs, P. and Van Hoorebeke, L., 2008. High-speed neutron radiography for monitoring the water absorption by capillarity in porous materials. Nuclear Instruments & Methods in Physics Research Section B-Beam Interactions with Materials and Atoms, 266(1): 155-163.

Cnudde, V., Silversmit, G., Boone, M., Dewanckele, J., De Samber, B., Schoonjans, T., Van Loo, D., De Witte, Y., Elburg, M., Vincze, L., Van Hoorebeke, L. and Jacobs, P., 2009. Multi-disciplinary characterisation of a sandstone surface crust. Science of the Total Environment, 407(20): 5417-5427.

Coenen, J., Tchouparova, E. and Jing, X., 2004. Measurement parameters and resolution aspects of micro X-ray tomography for advanced core analysis. Proceedings of International Symposium of the Society of Core Analysts, Abu Dhabi, UAE.

Coleou, C., Lesaffre, B., Brzoska, J.-B., Ludwig, W. and Boller, E., 2001. Three-dimensional snow images by X-ray microtomography Annals of Glaciology, 32(1): 75-81.

Coles, M.E., Hazlett, R.D., Spanne, P., Soll, W.E., Muegge, E.L. and Jones, K.W., 1998. Pore level imaging of fluid transport using synchrotron X-ray microtomography. Journal of Petroleum Science and Engineering, - 19(- 1-2): 55- 63.

Coles, M.E., Muegge, E.L. and Sprunt, E.S., 1991. Applications of CAT scanning for oil and gas-production research. IEEE Transactions on Nuclear Science, 38(2): 510-515.

Coles, M.E., Spanne, P., Muegge, E.L., Jones, K.W. and Soc Core, A., 1994. Computed microtomography of reservoir core samples. 1994 International Symposium of the Society of Core Analysts, Proceedings: 9-&.

Conroy, G.C. and Vannier, M.W., 1987. Dental development of the taung skull from coputerized-tomography. Nature, 329(6140): 625-627.

Crestana, S., Cesareo, R. and Mascarenhas, S., 1986. Using a computed tomography miniscanner in soil science. Soil Science, 142(1): 56-61.

Crestana, S., Mascarenhas, S. and Pozzimucelli, R.S., 1985. Static and dynamic 3-dimensional studies of water in soil using computed tomographic scanning. Soil Science, 140(5): 326-332.

Crowe, K.M., Budinger, T.F., Cahoon, J.L., Elischer, V.P., Huesman, R.H. and Kanstein, L.L., 1975. Axial scanning with 900 MeV alpha-particles. IEEE Transactions on Nuclear Science, 22(3): 1752-1754.

Dann, R., Turner, M., Close, M. and Knackstedt, M., 2011. Multi-scale characterisation of coastal sand aquifer media for contaminant transport using X-ray computed tomography. Environmental Earth Sciences, 63(5): 1125-1137.

David, C., Weitkamp, T., Pfeiffer, F., Diaz, A., Bruder, J., Rohbeck, T., Groso, A., Bunk, O., Stampanoni, M. and Cloetens, P., 2007. Hard X-ray phase imaging and tomography using a grating interferometer. Spectrochimica Acta, Part B: Atomic Spectroscopy, 62: 626-630.

De Man, B., Nuyts, J., Dupont, P., Marchal, G. and Suetens, P., 1998. Metal streak artifacts in X-ray computed tomography: a simulation study, Nuclear Science Symposium, Toronto, Canada, pp. 1860-1865.

De Witte, Y., 2010. Improved and practically feasible reconstruction methods for high resolution X-ray tomography, Ghent University, Ghent.

Defrise, M., Noo, F., Clackdoyle, R. and Kudo, H., 2006. Truncated Hilbert transform and image reconstruction from limited tomographic data. Inverse Problems, 22: 1037-1053.

Denison, C., Carlson, W.D. and Ketcham, R.A., 1997. Three-dimensional quantitative textural analysis of metamorphic rocks using high-resolution computed X-ray tomography .1. Methods and techniques. Journal of Metamorphic Geology, 15(1): 29-44.

Dewanckele, J., Cnudde, V., Boone, M., Van Loo, D., De Witte, Y., Pieters, K., Vlassenbroeck, J., Dierick, M., Masschaele, B., Van Hoorebeke, L. and Jacobs, P., 2009. Integration of X-ray micro tomography and fluorescence for applications on natural building stones. Journal of Physics: Conference Series, 186(1).

Dewanckele, J., De Kock, T., Boone, M.A., Cnudde, V., Brabant, L., Boone, M.N., Fronteau, G., Van Hoorebeke, L. and Jacobs, P., 2012. 4D imaging and quantification of pore structure modifications inside natural building stones by means of high resolution X-ray CT. Science of The Total Environment, 416: 436-448.

Dierick, M., Cnudde, V., Masschaele, B., Vlassenbroeck, J., Van Hoorebeke, L. and Jacobs, P., 2007. Micro-CT of fossils preserved in amber. Nuclear Instruments & Methods in Physics Research Section a-Accelerators Spectrometers Detectors and Associated Equipment, 580(1): 641-643.

Dierolf, M., Menzel, A., Thibault, P., Schneider, P., Kewish, C.M., Wepf, R., Bunk, O. and Pfeiffer, F., 2010. Ptychographic X-ray computed tomography at the nanoscale. Nature (London, United Kingdom), 467: 436-439.

Donoghue, P.C.J., Bengtson, S., Dong, X.-p., Gostling, N.J., Huldtgren, T., Cunningham, J.A., Yin, C., Yue, Z., Peng, F. and Stampanoni, M., 2006. Synchrotron X-ray tomographic microscopy of fossil embryos. Nature, 442: 680-683.

Dvorkin, J., Derzhi, N., Qian, F., Nur, A., Nur, B., Grader, A., Baldwin, C., Tono, H. and Diaz, E., 2009. From micro to reservoir scale: permeability from digital experiments. Leading Edge, 28(12).

Elliott, J.C. and Dover, S.D., 1982. X-ray microtomography. Journal of Microscopy - Oxford, 126: 211-213.

Elliott, J.C. and Dover, S.D., 1985. X-ray microscopy using computerized axial tomography. Journal of Microscopy - Oxford, 138(3): 329-331.

Ersoy, O., Sen, E., Aydar, E., Tatar, I. and Celik, H.H., 2010. Surface area and volume measurements of volcanic ash particles using micro-computed tomography (micro-CT): A comparison with scanning electron microscope (SEM) stereoscopic imaging and geometric considerations. Journal of Volcanology and Geothermal Research, 196(3-4): 281-286.

Feldkamp, L.A., Davis, L.C. and Kress, J.W., 1984. Practical cone-beam algorithm. Journal of the Optical Society of America A, 1(6): 612-619.

Feser, M., Gelb, J., Chang, H., Cui, H., Duewer, F., Lau, S.H., Tkachuk, A. and Yun, W., 2008. Sub-micron resolution CT for failure analysis and process development. Measurement Science & Technology, 19(9): 094001.

Firsching, M., 2009. Material Reconstruction in X-ray Imaging, Universität Erlangen-Nürnberg, Erlangen.

Flannery, B.P., Deckman, H.W., Roberge, W.G. and D'Amico, K.L., 1987. Three-dimensional X-ray microtomography. Science, 237(4821): 1439-1444.

Flin, F., Brzoska, J.-B., Lesaffre, B., Coleou, C. and Pieritz, R.A., 2004. Three-dimensional geometric measurements of snow microstructural evolution under isothermal conditions. Annals of Glaciology, 38(1): 39-44.

Flohr, T.G., McCollough, C.H., Bruder, H., Petersilka, M., Gruber, K., Süss, C., Grasruck, M., Stierstorfer, K., Krauss, B., Raupach, R., Primak, A.N., Küttner, A., Achenbach, S., Becker, C., Kopp, A. and Ohnesorge, B.M., 2006. First performance evaluation of a dual-source CT (DSCT) system. European Radiology, 16: 256-268.

Flohr, T.G., Raupach, R. and Bruder, H., 2009. Cardiac CT: How much can temporal resolution, spatial resolution, and volume coverage be improved. Journal of Cardiovascular Computed Tomography, 3: 143-152.

Frost, E.B., 1896. Experiments on the X-rays. Science, 3(59): 235-236.

Gai, Z., Donoghue, P.C.J., Zhu, M., Janvier, P. and Stampanoni, M., 2011. Fossil jawless fish from China foreshadows early jawed vertebrate anatomy. Nature (London, United Kingdom), 476: 324-327.

Gawler, J., Sanders, M.D., Bull, J.W.D., du Boulay, G. and Marshall, J., 1974. Computer assisted tomography in orbital disease. British Journal of Ophthalmology, 58: 571-587.

Gelb, J., Feser, M., Tkachuk, A., Hsu, G., Chen, S., Chang, H., Fong, T., Hunter, L., Goldberger, I., Lau, S.H. and Yun, W., 2009. Sub-micron X-ray computed tomography for non-destructive 3D visualization and analysis. Microscopy and Microanalysis, 15(Suppl 2): 618.

Geraud, Y., Mazerolle, F., Raynaud, S. and Lebon, P., 1998. Crack location in granitic samples submitted to heating, low confining pressure and axial loading. Geophysical Journal International, 133(3): 553-567.

Ghorbani, Y., Becker, M., Petersen, J., Morar, S.H., Mainza, A. and Franzidis, J.-P., 2011. Use of X-ray computed tomography to investigate crack distribution and mineral dissemination in sphalerite ore particles. Minerals Engineering, 24(12): 1249-1257.

Gilboy, W.B., 1984. X-ray and gamma-ray tomography in NDE applications. Nuclear Instruments & Methods in Physics Research, Section A: Accelerators, Spectrometers, Detectors, and Associated Equipment, 221(1): 193-200.

Gilboy, W.B., Foster, J. and Folkard, M., 1982. A tomographic gamma-ray scanner for industrial applications. Nuclear Instruments & Methods in Physics Research, Section A: Accelerators, Spectrometers, Detectors, and Associated Equipment, 193(1-2): 209-214.

Godard, P., Carbone, G., Allain, M., Mastropietro, F., Chen, G., Capello, L., Diaz, A., Metzger, T.H., Stangl, J. and Chamard, V., 2011. Three-dimensional high-resolution quantitative microscopy of extended crystals. Nature Communications, 2: 568.

Golab, A.N., Knackstedt, M.A., Averdunk, H., Senden, T., Butcher, A.R. and Jaime, P., 2010. 3D porosity and mineralogy characterization in tight gas sandstones. Leading Edge, 29(12).

Goldman, L.W., 2007. Principles of CT and CT technology. Journal of Nuclear Medicine Technology, 35(3): 115-128.

Grader, A.S., Clark, A.B.S., Al-Dayyani, T. and Nur, A., 2009. COMPUTATIONS OF POROSITY AND PERMEABILITY OF SPARIC CARBONATE USING MULTI-SCALE CT IMAGES. SCA2009-Temp Paper, International Symposium of the

Society of Core Analysts.

Graser, A., Johnson, T.R.C., Chandarana, H. and Macari, M., 2009. Dual-energy CT: preliminary observations and potential clinical applications in the abdomen. European Radiology, 19: 13-23.

Grochau, M.H., Campos, E., Nadri, D., Muumlller, T.M., Clennell, B. and Gurevich, B., 2010. Sedimentary cyclicity from X-ray CT images in Campos Basin, offshore Brazil. Leading Edge, 29(7): 808-813813.

Grodzins, L., 1983. Optimum energies for X-ray transmission tomography of small samples - Applications of synchrotron radiation to computerized-tomography. 1. Nuclear Instruments & Methods in Physics Research, Section A: Accelerators, Spectrometers, Detectors, and Associated Equipment, 206(3): 541-545.

Gualda, G.A.R., Pamukcu, A.S., Claiborne, L.L. and Rivers, M.L., 2010. Quantitative 3D petrography using X-ray tomography 3: Documenting accessory phases with differential absorption tomography. Geosphere, 6(6): 782-792.

Gualda, G.A.R. and Rivers, M., 2006. Quantitative 3D petrography using X-ray tomography: Application to Bishop Tuff pumice clasts. Journal of Volcanology and Geothermal Research, 154(1-2): 48-62.

Gy, P.M., 1976. The sampling of particulate materials --- a general theory. International Journal of Mineral Processing, 3: 289-312.

Haberthür, D., Hintermüller, C., Marone, F., Schittny, J.C. and Stampanoni, M., 2010. Radiation dose optimized lateral expansion of the field of view in synchrotron radiation X-ray tomographic microscopy. Journal of Synchrotron Radiation, 17(5): 590-599.

Hall, S.A., Bornert, M., Desrues, J., Pannier, Y., Lenoir, N., Viggiani, G. and Besuelle, P., 2010. Discrete and continuum analysis of localised deformation in sand using X-ray mu CT and volumetric digital image correlation. Geotechnique, 60(5): 315-322.

Hamblin, W.K., 1962. X-ray radiography in the study of structures in homogeneous sediments. Journal of Sedimentary Research, 32(2): 201-210.

Hanley, R. and Pavía, S., 2008. A study of the workability of natural hydraulic lime mortars and its influence on strength. Materials and Structures, 41(2): 373-381.

Hazlett, R.D., 1997. Statistical characterization and stochastic modeling of pore networks in relation to fluid flow. Mathematical Geology, 29(6): 801-822.

Heggli, M., Köchle, B., Matzl, M., Pinzer, B.R., Riche, F., Steiner, S., Steinfeld, D. and Schneebeli, M., 2011. Measuring snow in 3-D using X-ray tomography: assessment of visualization techniques. Annals of Glaciology, 52(58): 231-236.

Henderickx, H., Cnudde, V., Masschaele, B., Dierick, M., Vlassenbroeck, J. and Van Hoorebeke, L., 2006. Description of a new fossil Pseudogarypus (Pseudoscorpiones : Pseudogarypidae) with the use of X-ray micro-CT to penetrate opaque amber. Zootaxa(1305): 41-50.

Henderickx, H., Tafforeau, P. and Soriano, C., 2012. Phase-contrast synchrotron microtomography reveals the morphology of a partially visible new Pseudogarypus in Baltic amber (Pseudoscorpiones: Pseudogarypidae). Palaeontologia Electronica, 15(2).

Herm, D., 1973. Paleontology. Naturwissenschaften, 63(2): 81-86.

Herman, G.T., 1980. Image reconstruction frol projections: The fundamentals of computerized tomography. Computer science and applied mathematics. Academic Press, New York, 316 pp.

Herman, G.T. and Natterer, F., 1981. Mathematical aspects of computerized tomography. Springer-Verlag, 309 pp.

Hopkins, F.F., Morgan, I.L., Ellinger, H.D., Klinksiek, R.V., Meyer, G.A. and Thompson, J.N., 1981. Industrial tomography applications. IEEE Transactions on Nuclear Science, 28(2): 1717-1720.

Hounsfield, G.N., 1973. Computerized transverse axial scanning (tomography): Part I. Description of system. British Journal of Radiology, 46(552): 1016-1022.

Howard, J.D., 1968. X-ray radiography for examination of burrowing in sediments by marine invertebrate organisms. Sedimentology, 11(3-4): 249-258.

Iassonov, P., Gebrenegus, T. and Tuller, M., 2009. Segmentation of X-ray computed tomography images of porous materials: A crucial step for characterization and quantitative analysis of pore structures. Water Resources Research, 45: W09415.

Iglauer, S., Paluszny, A., Pentland, C.H. and Blunt, M.J., 2011. Residual CO2 imaged with X-ray micro-tomography Geophysical Research Letters, 38: L21403.

Ikeda, S., Nakano, T., Tsuchiyama, A., Uesugi, K., Suzuki, Y., Nakamura, K., Nakashima, Y. and Yoshida, H., 2004. Nondestructive three-dimensional element-concentration mapping of a Cs-doped partially molten granite by X-ray computed tomography using synchrotron radiation. American Mineralogist, 89(8-9): 1304-1313.

Ingham, J.P., 2005. Predicting the frost resistance of building stone. Quarterly Journal of Engineering Geology and Hydrogeology, 38: 387-399.

Ito, A. and Koyamaito, H., 1984. Possible use of proton CT as a means of density normalization in the PIXE semi-microprobe analysis. Nuclear Instruments & Methods in Physics Research, Section B: Beam Interactions with Materials and Atoms, 3(1-3): 584-588.

Jakubek, J., Holy, T., Jakubek, M., Vavrik, D. and Vykydal, Z., 2006. Experimental system for high resolution X-ray transmission radiography. Nuclear Instruments & Methods in Physics Research, Section A: Accelerators, Spectrometers, Detectors, and Associated Equipment, 563: 278-281.

Jerram, D.A., Mock, A., Davis, G.R., Field, M. and Brown, R.J., 2009. 3D crystal size distributions: A case study on quantifying olivine populations in kimberlites. Lithos, 112: 223-235.

Kaempfer, T.U., Schneebeli, M. and Sokratov, S.A., 2005. A microstructural approach to model heat transfer in snow. Geophysical Research Letters, 32: L21503.

Kak, A.C. and Slaney, M., 1988. Principles op computerized tomographic imaging. IEEE Press, New York, 329 pp.

Kalam, Z., Al Dayyani, T., Grader, A. and Sisk, C., 2011. Digital rock physics analysis in complex carbonates. World Oil, 234(5).

Karacan, C.O. and Mitchell, G.D., 2003. Behavior and effect of different coal microlithotypes during gas transport for carbon dioxide sequestration into coal seams. International Journal of Coal Geology, 53(4): 201-217.

Karpyn, Z.T., Alajmi, A., Radaelli, F., Halleck, P.M. and Grader, A.S., 2009. X-ray CT and hydraulic evidence for a relationship between fracture conductivity and adjacent matrix porosity. Engineering Geology, 103(3-4): 139-145.

Keller, A., 1998. High resolution, non-destructive measurement and characterization of fracture apertures. International Journal of Rock Mechanics and Mining Sciences, 35(8): 1037-1050.

Keller, A.A., Roberts, P.V. and Blunt, M.J., 1999. Effect of fracture aperture variations on the dispersion of contaminants. Water Resources Research, 35(1): 55-63.

Kerckhofs, G., Schrooten, J., Van Cleynenbreugel, T., Lomov, S.V. and Wevers, M., 2008. Validation of x-ray microfocus computed tomography as an imaging tool for porous structures. Review of Scientific Instruments, 79: 013711.

Kervyn, M., Boone, M.N., de Vries, B.v.W., Lebas, E., Cnudde, V., Fontijn, K. and Jacobs, P., 2010. 3D imaging of volcano gravitational deformation by computerized X-ray micro-tomography. Geosphere, 6(5): 482-498.

Ketcham, R.A., 2005. Computational methods for quantitative analysis of three-dimensional features in geologic specimens. Geosphere, 1: 32-41.

Ketcham, R.A. and Carlson, W.D., 2001. Acquisition, optimization and interpretation of X-ray computed tomographic imagery: applications to the geosciences. Computers & Geosciences, 27(4): 381-400.

Ketcham, R.A. and Iturrino, G.J., 2005. Nondestructive high-resolution visualization and measurement of anisotropic effective porosity in complex lithologies using high-resolution X-ray computed tomography. Journal of Hydrology, 302(1-4): 92-106.

Ketcham, R.A., Slottke, D.T. and Sharp, J.M., 2010. Three-dimensional measurement of fractures in heterogeneous materials using high-resolution X-ray computed tomography. Geosphere, 6(5): 499-514.

Knoll, G.F., 2000. Radiation Detection and Measurement. J. Wiley & Sons.

Koch, A., Raven, C., Spanne, P. and Snigirev, A., 1998. X-ray imaging with submicrometer resolution employing transparent luminescent screens. Journal of the Optical Society of America A, Optics and Image Science, 15(7): 1940-1951.

Koeppe, R.A., Brugger, R.M., Schlapper, G., A., Larsen, G.N. and Jost, R.J., 1981. Neutron Computed Tomography. Journal of Computer Assisted Tomography, 5(1): 79-88.

Kumar, M., Senden, T.J., Sheppard, A.P., Middleton, J.P. and Knackstedt, M.A., 2010a. Visualizing and Quantifying the Residual Phase Distribution in Core Material. Petrophysics, 51(5): 323-332.

Kumar, M., Sok, R., Knackstedt, M.A., Latham, S., Senden, T.J., Sheppard, A.P., Varslot, T. and Arns, C., 2010b. Mapping 3D Pore Scale Fluid Distributions: How Rock Resistivity is Influenced by Wettability and Saturation History. Petrophysics, 51(2): 102-117.

Kyle, J.R., Mote, A.S. and Ketcham, R.A., 2008. High resolution X-ray computed tomography studies of Grasberg porphyry Cu-Au ores, Papua, Indonesia. Mineralium Deposita, 43(5): 519-532.

Kyrieleis, A., Titarenko, V., Ibison, M., Connolley, T. and Withers, P.J., 2011. Region-of-interest tomography using filtered backprojection: assessing the practical limits. Journal of Microscopy, 241(1): 69-82.

Lanas, J., Bernal, J.L.P., Bello, M.A. and Galindo, J.I.A., 2004. Mechanical properties of natural hydraulic lime-based mortars. Cement and Concrete Research, 34(12): 2191-2201.

Latief, F.D.E., Biswal, B., Fauzi, U. and Hilfer, R., 2010. Continuum reconstruction of the pore scale microstructure for Fontainebleau sandstone. Physica A, 389(8): 1607-1618.

Ledley, R.S., Dichiro, G., Luessenh, A.J. and Twigg, H.L., 1974. Computerize transaxial tomography of human body. Science, 186(4160): 207-212.

Lehmann, E.H. and Wagner, W., 2010. Neutron imaging at PSI: a promising tool in materials science and technology. Applied Physics A, 99: 627-634.

Lenoir, N., Bornert, M., Desrues, J., Bésuelle, P. and Viggiani, G., 2007. Volumetric Digital Image Correlation Applied to X-ray Microtomography Images from Triaxial Compression Tests on Argillaceous Rock. Strain, 43(3): 193-205.

Lenoir, N., Marello, S., Viggiani, G., Besuelle, P., Desrues, J. and Di Michiel, M., 2004. X-ray micro tomography characterization of strain localization upon deviatoric loading of saturated fine-grained stiff soils. X-Ray Ct for Geomaterials Soils, Concrete, Rocks, 147-155 pp.

Lesher, C.E., Wang, Y.B., Gaudio, S., Clark, A., Nishiyama, N. and Rivers, M., 2009. Volumetric properties of magnesium silicate glasses and supercooled liquid at high pressure by X-ray microtomography. Physics of the Earth and Planetary Interiors, 174(1-4): 292-301.

Lindquist, W.B., 2001. Quantitative analysis of three dimensional X-ray tomographic images. In: U. Bonse (Editor), 3rd Conference on Developments in X-Ray Tomography. SPIE-INT SOC OPTICAL ENGINEERING, San Diego, CA, pp. 103-115.

Louis, L., Wong, T.-F. and Baud, P., 2007. Imaging strain localization by X-ray radiography and digital image correlation: Deformation bands in Rothbach sandstone. Journal of Structural Geology, 29(1): 129-140.

Maravelaki-Kalaitzaki, P., Bakolas, A., Karatasios, I. and Kilikoglou, V., 2005. Hydraulic lime mortars for the restoration of historic masonry in Crete. Cement and Concrete Research, 35(8): 1577-1586.

Masad, E., Saadeh, S., Al-Rousan, T., Garboczi, E. and Little, D., 2005. Computations of particle surface characteristics using optical and X-ray CT images. Computational Materials Science, 34(4): 406-424.

Masschaele, B., Cnudde, V., Dierick, M., Jacobs, P., Van Hoorebeke, L. and Vlassenbroeck, J., 2007. UGCT: New X-ray radiography and tomography facility. Nuclear Instruments & Methods in Physics Research, Section A: Accelerators, Spectrometers, Detectors, and Associated Equipment, 580: 266-269.

McCoy, T.J., Ketcham, R.A., Wilson, L., Benedix, G.K., Wadhwa, M. and Davis, A.M., 2006. Formation of vesicles in asteroidal basaltic meteorites. Earth and Planetary Science Letters, 246(1-2): 102-108.

Miller, D.C., 1896. Röntgen ray experiments. Science, 3(66): 516-517.

Minter, N.J., Franks, N.R. and Brown, K.A.R., 2012. Morphogenesis of an extended phenotype: four-dimensional ant nest architecture. Journal of the Royal Society Interface, 9(68): 586-595.

Mokso, R., Marone, F., Haberthür, D., Schittny, J.C., Mikuljan, G., Isenegger, A. and Stampanoni, M., 2011. Following Dynamic Processes by X-ray Tomographic Microscopy with Sub-second Temporal Resolution. In: I. McNulty, C. Eyberger and B. Lai (Editors), 10TH INTERNATIONAL CONFERENCE ON X-RAY MICROSCOPY, pp. 38-41.

Mokso, R., Quaroni, L., Marone, F., Irvine, S., Vila-Comamala, J., Blanke, A. and Stampanoni, M., 2012. X-ray mosaic nanotomography of large microorganisms. Journal of Structural Biology, 177(2): 233-238.

Monna, F., Lancelot, J., Bernat, M. and Mercadier, H., 1997. Sedimentation rate in the Thau basin (France) according to geochronological, geochemical and stratigraphical data. Oceanologica Acta, 20(4): 627-638.

Murphy, W.A., zur Nedden, D., Gostner, P., Knapp, R., Rechels, W. and Seldler, H., 2003. The Iceman: discovery and imaging. Radiology, 226: 614-629.

Nakashima, Y., Kamiya, S. and Nakano, T., 2008. Diffusion ellipsoids of anisotropic porous rocks calculated by X-ray computed tomography-based random walk simulations. Water Resources Research, 44(12).

Navarre-Sitchler, A., Steefel, C.I., Yang, L., Tomutsa, L. and Brantley, S.L., 2009. Evolution of porosity and diffusivity associated with chemical weathering of a basalt clast. Journal of Geophysical Research-Earth Surface, 114.

Ohno, Y., Kohno, T., Matsufuji, N. and Kanai, T., 2004. Measurement of electron density distribution using heavy ion CT. Nuclear Instruments & Methods in Physics Research, Section B: Beam Interactions with Materials and Atoms, 525(1-2): 279-283.

Okui, T., Uchida, T. and Masuda, Y., 2003. Observation of natural gas hydrate dissociation with X-ray CT. In: J. Otani and Y. Obara (Editors), International Workshop on X-Ray CT for Geomaterials (GeoX 2003), Kumamoto, JAPAN, pp. 347-351.

Ommaya, A.K., Murray, G., Ambrose, J., Richardson, A. and Hounsfield, G.N., 1976. Computerized axial tomography: estimation of spatial and density resolution capability. British Journal of Radiology, 49: 604-611.

Onoe, M., Tsao, J.W., Yamada, H., Nakamura, H., Kogure, J., Kawamura, H. and Yoshimatsu, M., 1983. Computed-tomography for measuring annual rings of a live tree. Proceedings of the IEEE, 71(7): 907-908.

Øren, P.E. and Bakke, S., 2002. Process Based Reconstruction of Sandstones and Prediction of Transport Properties. Transport in Porous Media 46: 311–343.

Orsi, T.H., Edwards, C.M. and Anderson, A.L., 1994. X-RAY COMPUTED-TOMOGRAPHY - A NONDESTRUCTIVE METHOD FOR QUANTITATIVE-ANALYSIS OF SEDIMENT CORES. Journal of Sedimentary Research Section a-Sedimentary Petrology and Processes, 64(3): 690-693.

Otani, J., Watanabe, Y. and Chevalier, B., 2010. Introduction of X-ray CT application in geotechnical engineering - theory and practice. In: N.V.S.L.Q.R.A. Khalili (Editor), 9th World Congress on

Computational Mechanics and 4th Asian Pacific Congress on Computational Mechanics. IOP Conference Series-Materials Science and Engineering.

Overley, J.C., 1983. Element-sensitive computed tomography with fast neutrons. Journal of Computer Assisted Tomography, 7(1): 117-125.

Passmore, M.S., Bates, R., Mathieson, K., O'Shea, V., Rahman, M., Seller, P. and Smith, K.M., 2001. Characterisation of a single photon counting pixel detector. Nuclear Instruments & Methods in Physics Research, Section A: Accelerators, Spectrometers, Detectors, and Associated Equipment, 466: 202-208.

Paxton, R. and Ambrose, J., 1974. The EMI scanner. A brief review of the first 650 patients. British Journal of Radiology, 47: 430-565.

Penney, D., Dierick, M., Cnudde, V., Masschaele, B., Vlassenbroeck, J., Van Hoorebeke, L. and Jacobs, P., 2007. First fossil micropholcommatidae (Araneae), imaged in eocene Paris amber using x-ray computed tomography. Zootaxa(1623): 47-53.

Perreau, M. and Tafforeau, P., 2011. Virtual dissection using phase-contrast X-ray synchrotron microtomography: reducing the gap between fossils and extant species. Systematic Entomology, 36(3): 573-580.

Perrichot, V., Engel, M.S., Nel, A., Tafforeau, P. and Soriano, C., 2011. New earwig nymphs (Dermaptera: Pygidicranidae) in mid-Cretaceous amber from France. Cretaceous research, 32(3): 325-330.

Petchsingto, T. and Karpyn, Z.T., 2009. Deterministic Modeling of Fluid Flow through a CT-scanned Fracture Using Computational Fluid Dynamics. Energy Sources Part a-Recovery Utilization and Environmental Effects, 31(11): 897-905.

Peth, S., 2010. Applications of microtomography in soils and sediments. In: B. Singh and M. Gräfe (Editors), Developments in Soil Science. ELSEVIER, pp. 73-101.

Peth, S., Nellesen, J., Fischer, G. and Horn, R., 2010. Non-invasive 3D analysis of local soil deformation under mechanical and hydraulic stresses by mu CT and digital image correlation. Soil & Tillage Research, 111(1): 3-18.

Petrovic, A.M., Siebert, J.E. and Rieke, P.E., 1982. Soil bulk-density analysis in 3 dimensions by computed tomographic scanning. Soil Science Society of America Journal, 46(3): 445-450.

Pfeiffer, K.-F.G., 2004. Evaluation of the Medipix detectors for medical X-ray imaging, with special consideration of mammography, Universität Erlangen, Nürnberg.

Pieritz, R.A., Brzoska, J.-B., Flin, F., Lesaffre, B. and Coléou, C., 2004. From snow X-ray microtomograph raw volume data to micromechanics modeling: first results Annals of Glaciology, 38(1): 52-58.

Pirlet, H., Wehrmann, L.M., Brunner, B., Frank, N., Dewanckele, J., Van Rooij, D., Foubert, A., Swennen, R., Naudts, L., Boone, M., Cnudde, V. and Henriet, J.-P., 2010. Diagenetic formation of gypsum and dolomite in a cold-water coral mound in the Porcupine Seabight, off Ireland. Sedimentology, 57(3): 786-805.

Pirlet, H., Wehrmann, L.M., Foubert, A., Brunner, B., Blamart, D., De Mol, L., Van Rooij, D., Dewanckele, J., Cnudde, V., Swennen, R., Duyck, P. and Henriet, J.-P., 2012. Unique authigenic mineral assemblages reveal different diagenetic histories in two neighbouring cold-water coral mounds on Pen Duick Escarpment, Gulf of Cadiz. Sedimentology, 59(2): 578-604.

Polacci, M., Baker, D.R., Mancini, L., Tromba, G. and Zanini, F., 2006. Three-dimensional investigation of volcanic textures by X-ray microtomography and implications for conduit processes. Geophysical Research Letters, 33(13).

Polacci, M., Burton, M.R., La Spina, A., Mure, F., Favretto, S. and Zanini, F., 2009. The role of syn-eruptive vesiculation on explosive basaltic activity at Mt. Etna, Italy. Journal of Volcanology and Geothermal Research, 179(3-4): 265-269.

Polacci, M., Mancini, L. and Baker, D.R., 2010. The contribution of synchrotron X-ray computed microtomography to understanding volcanic processes. Journal of Synchrotron Radiation, 17: 215-221.

Polak, A., Elsworth, D., Yasuhara, H., Grader, A.S. and Halleck, P.M., 2003. Permeability reduction of a natural fracture under net dissolution by hydrothermal fluids. Geophysical Research Letters, 30(20).

Primak, A.N., Fletcher, J.G., Vrtiska, T.J., Dzyubak, O.P., Lieske, J.C., Jockson, M.E., Williams, J.C.J. and McCollough, C.H., 2007. Noninvasive differentiation of uric acid versus non-uric acid kidney stones using dual-energy CT. Academic Radiology, 14(12): 1441-1447.

Purcell, C., Harbert, W., Soong, Y., McLendon, T.R., Haljasmaa, I.V., McIntyre, D. and JiKich, J., 2009. Velocity measurements in reservoir rock samples from the SACROC unit using various pore fluids, and integration into a seismic survey taken before and after a CO2 sequestration flood. In: J. Gale, H. Herzog and J. Braitsch (Editors), Greenhouse Gas Control Technologies 9. Energy Procedia. Elsevier Science Bv, Amsterdam, pp. 2323-2331.

PyrakNolte, L.J., Montemagno, C.D. and Nolte, D.D., 1997. Volumetric imaging of aperture distributions in connected fracture networks. Geophysical Research Letters, 24(18): 2343-2346.

Qi, X.Z., Zhao, J., Xiao, C.W. and Liu, R.L., 2000. A study on the quantitative processing methods of image data. Proceedings of SPE International Oil and Gas Conference and Exhibition, SPE 64626: 7-11.

Raynaud, S., Vasseur, G., Celerier, B., Loggia, D., Ghoreychi, M., Mathon, M.H. and Mazerolle, F., 2010. Experimental study of the relation between the permeability of kaolinite and its deformation at micro and macro scale. International Journal of Rock Mechanics and Mining Sciences, 47(4): 559-567.

Redwan, M. and Rammlmair, D., 2010. Simultaneous monitoring of water saturation and fluid conductivity in unconsolidated sand columns. Soil Science Society of America Journal, 74(5): 1457-1468.

Remeysen, K. and Swennen, R., 2008. Application of microfocus computed tomography in carbonate reservoir characterization: Possibilities and limitations. Marine and Petroleum Geology, 25(6): 486-499.

Ribeiro, J.L.B., Lopes, R.T., Anjos, M.J., Queiroz Neto, J.C., Bianco, L.C.B., Campos, E.F. and D'Almeida, A.R., 2007a. Study of performance with diverting agents in formation damage and return of permeability for unconsolidated sandstones using computed tomography, 2006 IEEE Nuclear Science Symposium Conference Record. Ieee, San Diego, CA,, pp. 7 pp.-7 pp.

Ribeiro, J.L.B., Quelroz, J.C., Lopes, R.T., Anjos, M.J., Blanco, L.C.B., D'Almeida, A.R. and Campos, E.F., 2007b. New methodology for analysis of performance for diverting agents in unconsolidated sandstones in real time with physical simulator using computed tomography. Nuclear Instruments & Methods in Physics Research Section a-Accelerators Spectrometers Detectors and Associated Equipment, 579(1): 481-485.

Ritman, E.L., 2004. Micro-computed tomography - Current status and developments. Annual Review of Biomedical Engineering, 6: 185-208.

Rivers, M.L., Wang, Y.B. and Uchida, T., 2004. Microtomography at GeoSoilEnviroCARS. In: U. Bonse (Editor), Developments in X-Ray Tomography Iv. Proceedings of the Society of Photo-Optical Instrumentation Engineers (Spie). Spie-Int Soc Optical Engineering, Bellingham, pp. 783-791.

Rizzo, G. and Megna, B., 2008. Characterization of hydraulic mortars by means of simultaneous thermal analysis. Journal of Thermal Analysis and Calorimetry, 92(1): 173-178.

Rozenbaum, O., 2011. 3-D characterization of weathered building limestones by high resolution synchrotron X-ray microtomography. Science of the Total Environment, 409(10): 1959-1966.

Saadatfar, M., Sheppard, A.P., Senden, T.J. and Kabla, A.J., 2012. Mapping forces in a 3D elastic assembly of grains. Journal of the Mechanics of Physics and Solids, 60(1): 55-66.

Sakellariou, A., Kingston, A.M., Varslot, T.K., Sheppard, A.P., Latham, S.J., Sok, R.M., Arns, C.H., Senden, T.J. and Knackstedt, M.A., 2010. Tomographic image analysis and processing to simulate micro-petrophysical experiments. In: S.R. Stock (Editor), Developments in X-Ray Tomography Vii. Proceedings of SPIE-The International Society for Optical Engineering.

Santos, L.O.E., Philippi, P.C., Damiani, M.C. and Fernandes, C.P., 2002. Using three-dimensional reconstructed microstructures for predicting intrinsic permeability of reservoir rocks based on a Boolean lattice gas method. J. Petrol. Sci. Eng., 35: 109-124.

Sasov, A. and Van Dyck, D., 1998. Desktop X-ray microscopy and microtomography. Journal of Microscopy - Oxford, 191: 151-158.

Sato, T., Ikeda, O., Yamakoshi, Y. and Tsubouchi, M., 1981. X-ray tomography for microstructural objects. Applied Optics, 20(22): 3880-3883.

Schlindelin, J., Arganda-Carreras, I., Frise, E., Kaynig, V., Longair, M., Petzsch, T., Preibisch, S., Rueden, C., Saalfeld, S., Schmid, B., Tenevez, J.-Y., White, D.J., Hartenstein, V., Eliceiri, K., Tomancak, P. and Cardona, A., 2012. Fiji: an open-source platform for biological-image analysis Nature Methods, 9(7): 676-682.

Schmidt, S., Jouanneau, J.-M., Weber, O., Lecroart, P., Radakovitch, O., Gilbert, F. and Jézéquel, D., 2007. Sedimentary processes in the Thau Lagoon (France): From seasonal to century time scales. Estuarine, Coastal and Shelf Science, 72(3): 534-542.

Schneebeli, M. and Sokratov, S.A., 2004. Tomography of temperature gradient metamorphism of snow and associated changes in heat conductivity. Hydrological Processes, 18(18): 3655-3665.

Schropp, A., Hoppe, R., Patommel, J., Samberg, D., Seiboth, F., Stephan, S., Wellenreuther, G., Falkenberg, G. and Schroer, C.G., 2012. Hard x-ray scanning microscopy with coherent radiation: Beyond the resolution of conventional x-ray microscopes. Applied Physics Letters, 100(25): 253112.

Schuster, D.P., Kovacs, A., Garbow, J. and Piwnica-Worms, D., 2004. Recent advances in imaging the lungs of intact small animals. American Journal of Respiratory Cell and Molecular Biology, 30(2): 129-138.

Shinoda, H., Kanai, T. and Kohno, T., 2006. Application of heavy-ion CT. Physics in Medicine and Biology, 51: 4073-4081.

Siddiqui, S., Funk, J.J. and Al-Tahini, A.M., 2010. Use of X-Ray CT To Measure Pore Volume Compressibility of Shaybah Carbonates. Spe Reservoir Evaluation & Engineering, 13(1): 155-164.

Siewerdsen, J.H. and Jaffray, D.A., 1999. Cone-beam computed tomography with a flat-panel imager: Effects of image lag. Medical Physics, 26(12): 2635-2647.

Sijbers, J. and Postnov, A., 2004. Reduction of ring artefacts in high resolution micro-CT reconstructions. Physics in Medicine and Biology, 49: N247-N253.

Silin, D., Tomutsa, L., Benson, S.M. and Patzek, T.W., 2011. Microtomography and pore-scale modelling of two-phase fluid distribution. Transport in Porous Media, 86(2): 495-515.

Singh, K., Niven, R.K., Senden, T.J., Turner, M.L., Sheppard, A.P., Middleton, J.P. and Knackstedt, M.A., 2011. Remobilization of Residual Non-Aqueous Phase Liquid in Porous Media by Freeze-Thaw Cycles. Environmental Science & Technology, 45(8): 3473-3478.

Sleutel, S., Cnudde, V., Masschaele, B., Vlassenbroeck, J., Dierick, M., Van Hoorebeke, L., Jacobs, P. and De Neve, S., 2008. Comparison of different nano- and micro-focus X-ray computed tomography set-ups for the visualization of the soil microstructure and soil organic matter. Computers & Geosciences, 34(8): 931-938.

Sok, R.M., Varslot, T., Ghous, A., Latham, S., Sheppard, A.P. and Knackstedt, M.A., 2010. Pore Scale Characterization of Carbonates at Multiple Scales: Integration of Micro-CT, BSEM, and FIBSEM. Petrophysics, 51(6): 379-387.

Spanne, P., Jones, K.W., Prunty, L. and Anderson, S.H., 1994a. POTENTIAL APPLICATIONS OF SYNCHROTRON COMPUTED MICROTOMOGRAPHY TO SOIL SCIENCE. In: S.H.H.J.W. Anderson (Editor), Tomography of Soil-Water-Root Processes. Sssa Special Publications, pp. 43-57.

Spanne, P., Thovert, J.F., Jacquin, C.J., Lindquist, W.B., Jones, K.W. and Adler, P.M., 1994b. SYNCHROTRON COMPUTED MICROTOMOGRAPHY OF POROUS-MEDIA - TOPOLOGY AND TRANSPORTS. Physical Review Letters, 73(14): 2001-2004.

Speijer, R.P., Van Loo, D., Masschaele, B., Vlassenbroeck, J., Cnudde, V. and Jacobs, P., 2008. Quantifying foraminiferal growth with high-resolution X-ray computed tomography: New opportunities in foraminiferal ontogeny, phylogeny, and paleoceanographic applications. Geosphere, 4(4): 760-763.

Stampanoni, M., Borchert, G., Wyss, P., Abela, R., Patterson, B., Hunt, S., Vermeulen, D. and Rüegsegger, P., 2002. High resolution X-ray detector for synchrotron-based microtomography. Nuclear Instruments & Methods in Physics Research Section a-Accelerators Spectrometers Detectors and Associated Equipment, 491(1-2): 291-301.

Stampanoni, M., Groso, A., Isenegger, A., Mikuljan, G., Chen, Q., Bertrand, A., Henein, S., Betemps, R., Frommherz, U., Böhler, P., Meister, D., Lange, M. and Abela, R., 2006. Trens in synchrotron-based tomographic imaging: the SLS experience. In: U. Bonse (Editor), Developments in X-ray Tomography V. Proc. SPIE, San Diego, CA, USA, pp. 63180M.

Sturmer, W., 1973. X-ray photography in paleontology - some new results. Naturwissenschaften, 60(9): 407-411.

Szemerey-Kiss, B. and Török, Á., 2011. Time-dependent changes in the strength of repair mortar used in the loss compensation of stone. Environmental Earth Sciences, 63(7): 1613-1621.

Tafforeau, P., Boistel, R., Boller, E., Bravin, A., Brunet, M., Chaimanee, Y., Cloetens, P., Feist, M., Hoszowska, J., Jaeger, J.-J., Kay, R.F., Lazzari, V., Marivauw, L., Nel, A., Nemoz;C., Thibault, X., Vignaud, P. and Zabler, S., 2006. Applications of X-ray synchrotron microtomography for non-destructive 3D studies of paleontological specimens. Applied Physics A, 83: 195-202.

Takada, Y., Kondo, K., Marume, T., Nagayoshi, K., Okada, I. and Takikawa, K., 1988. Proton computed-tomography with a 250 MeV pulsed-beam. Nuclear Instruments & Methods in Physics Research, Section A: Accelerators, Spectrometers, Detectors, and Associated Equipment, 273(1): 410-422.

Tarplee, M.F.V., van der Meer, J.J.M. and Davis, G.R., 2011. The 3D microscopic 'signature' of strain within glacial sediments revealed using X-ray computed microtomography. Quaternary Science Reviews, 30(23-24): 3501-3532.

Taylor, F.W., Wagner, F.G., McMillin, C.W., Morgan, I.L. and Hopkins, F.F., 1984. Location knots by industrial tomography - A feasability study. Forest Products Journal, 34(5): 42-46.

Tlustos, L., Campbell, M., Heijne, E. and Llopart, X., 2004. Signal variations in high-granularity Si pixel detectors. IEEE Transactions on Nuclear Science, 51(6): 3006-3012.

Török, A. and Prikryl, R., 2010. Current methods and future trends in testing, durability analyses and provenance studies of natural stones used in historical monuments. Engineering Geology, 115(3-4): 139-142.

Toumllke, J., Baldwin, C., Yaoming, M., Derzhi, N., Qian, F., Grader, A. and Dvorkin, J., 2010. Computer simulations of fluid flow in sediment: from images to permeability. Leading Edge, 29(1).

Turbell, H., 2001. Cone-beam reconstruction using filtered backprojection, Linköping University, Linköping.

Uchida, T., Dallimore, S. and Mikami, J., 2000. Occurrences of natural gas hydrates beneath the permafrost zone in Mackenzie Delta - Visual and X-ray CT imagery. In: G.D.B.P.R. Holder (Editor), Gas Hydrates: Challenges for the Future. Annals of the New York Academy of Sciences, pp. 1021-1033.

Van de Casteele, E., Van Dyck, D., Sijbers, J. and Raman, E., 2002. An energy-based beam hardening model in tomography. Physics in Medicine and Biology, 47: 4181-4190.

Van den Bulcke, J., Boone, M.N., Van Acker, J. and Van Hoorebeke, L., 2009. Three-dimensional X-ray imaging and analysis of fungi on and in wood. Microscopy and Microanalysis, 15(5): 395-402.

Van Rooij, D., Blamart, D., De Mol, L., Mienis, F., Pirlet, H., Wehrmann, L.M., Barbieri, R., Maignien, L., Templer, S.P., de Haas, H., Hebbeln, D., Frank, N., Larmagnat, S., Stadnitskaia, A., Stivaletta, N., van Weering, T., Zhang, Y., Hamoumi, N., Cnudde, V., Duyck, P., Henriet, J.P. and Mi, C.M.D.S.P., 2011. Cold-water coral mounds on the Pen Duick Escarpment, Gulf of Cadiz: The MICROSYSTEMS project approach. Marine Geology, 282(1-2): 102-117.

Vazquez-Calvo, C., De Buergo, M.A., Fort, R. and Varas, M.J., 2007. Characterization of patinas by means of microscopic techniques. Materials Characterization, 58(11-12): 1119-1132.

Viggiani, G., Lenoir, N., Besuelle, P., Di Michiel, M., Marello, S., Desrues, J. and Kretzschmer, M., 2004. X-ray microtomography for studying localized deformation in fine-grained geomaterials under triaxial compression. Comptes Rendus Mecanique, 332(10): 819-826.

Vinegar, H.J. and Wellington, S.L., 1987. Tomographic imaging of three-phase flow experiments. Review of Scientific Instruments, 58(1): 96-107.

Vlassenbroeck, J., 2009. Advances in laboratory-based X-ray microtomography, Ghent University, Ghent.

Vlassenbroeck, J., Dierick, M., Masschaele, B., Cnudde, V., Van Hoorebeke, L. and Jacobs, P., 2007. Software tools for quantification of X-ray microtomography at the UGCT. Nuclear Instruments & Methods in Physics Research, Section A: Accelerators, Spectrometers, Detectors, and Associated Equipment, 580: 442-445.

Voltolini, M., Marinoni, N. and Mancini, L., 2011. Synchrotron X-ray computed microtomography investigation of a mortar affected by alkali-silica reaction: a quantitative characterization of its microstructural features. Journal of Materials Science, 46(20): 6633-6641.

Watanabe, N., Ishibashi, T., Hirano, N., Tsuchiya, N., Ohsaki, Y., Tamagawa, T., Tsuchiya, Y. and Okabe, H., 2011a. Precise 3D Numerical Modeling of Fracture Flow Coupled With X-Ray Computed Tomography for Reservoir Core Samples. Spe Journal, 16(3): 683-691.

Watanabe, N., Ishibashi, T., Ohsaki, Y., Tsuchiya, Y., Tamagawa, T., Hirano, N., Okabe, H. and Tsuchiya, N., 2011b. X-ray CT based numerical analysis of fracture flow for core samples under various confining pressures. Engineering Geology, 123(4): 338-346.

Watanabe, Y., Otani, J., Lenoir, N. and Nakai, T., 2009. Evaluation of shear strain in sand under triaxial compression using CT data. Prediction and Simulation Methods for Geohazard Mitigation, 361-365 pp.

Weinekoetter, C., 2008. X-Ray Nanofocus CT: Visualising Of Internal 3D-Structures With Submicrometer Resolution. In: P. Munshi (Editor), Ct 2008: Tomography Confluence. Aip Conference Proceedings. Amer Inst Physics, Melville, pp. 3-14.

Weitkamp, T., Haas, D., Wegrzynek, D. and Rack, A., 2011. ANKAphase: software for single-distance phase retrieval from inline X-ray phase-contrast radiographs. Journal of Synchrotron Radiation, 18: 617-629.

Wellington, S.L. and Vinegar, H.J., 1987. X-RAY COMPUTERIZED-TOMOGRAPHY. Journal of Petroleum Technology, 39(8): 885-898.

Wennberg, O.P., Rennan, L. and Basquet, R., 2009. Computed tomography scan imaging of natural open fractures in a porous rock; geometry and fluid flow. Geophysical Prospecting, 57(2): 239-249.

Wildenschild, D. and Sheppard, A.P., 2012. X-ray imaging and analysis techniques for quantifying pore-scale structure and processes in subsurface porous medium systems. Advances in Water Resources.

Wilkins, S.W., Gureyev, T.E., Gao, D., Pogany, A. and Stevenson, A.W., 1984. Phase-contrast imaging using polychromatic hard X-rays. Nature, 384: 335-338.

Xin, Z., Schwartz, L.M., Tokso uml z, M.N., Smith, W.C. and Morgan, F.D., 2010. Pore-scale modeling of electrical and fluid transport in Berea sandstone. Geophysics, 75(5): F135-F142.

Young, P.G., Beresford-West, T.B.H., Coward, S.R.L., Notarberardine, B., Walker, B. and Abdul-Aziz, A., 2008. An efficient approach to converting three-dimensional image data into highly accurate computational models. Philosophical Transactions of the Royal Society of London, Series A: Physical Sciences and Engineering, 366: 3155-3173.

Zabler, S., Rack, A., Manke, I., Thermann, K., Tiedemann, J., Narthill and Riesemeier, H., 2008. High-resolution tomography of cracks, voids and micro-structure in greywacke and limestone. Journal of Structural Geology, 30(7): 876-887.

Zamyatin, A.A., Taguchi, K. and Silver, M.D., 2005. Helical cone beam CT with an asymmetrical detector. Medical Physics, 32(10): 3117-3127.

Zhu, W.C., Liu, J., Elsworth, D., Polak, A., Grader, A., Sheng, J.C. and Liu, J.X., 2007. Tracer transport in a fractured chalk: X-ray CT characterization and digital-image-based (DIB) simulation. Transport in Porous Media, 70(1): 25-42.

Zollikofer, C.P.E., de León, M.S.P. and Martin, R.D., 1998. Computer-assisted paleoanthropology. Evolutionary Anthropology, 6(2): 41-54.

Figure 1A

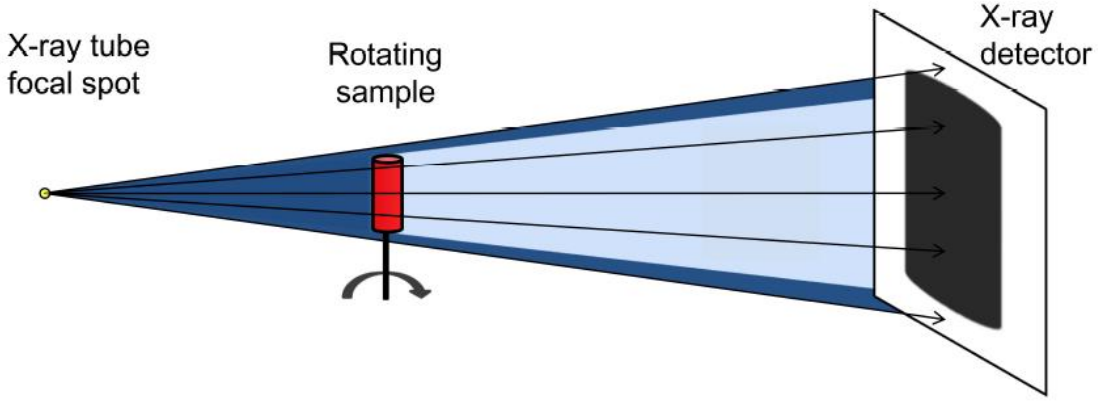

Figure 1B

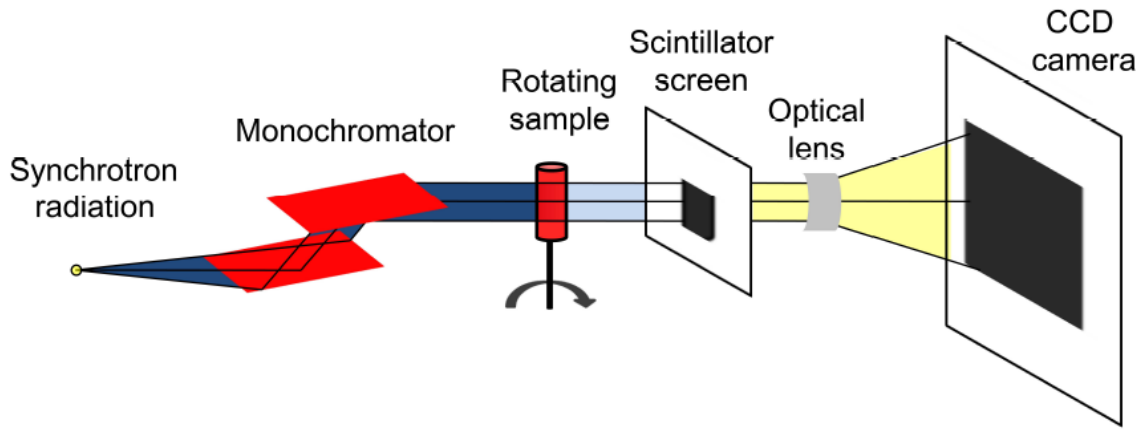

Figure 2

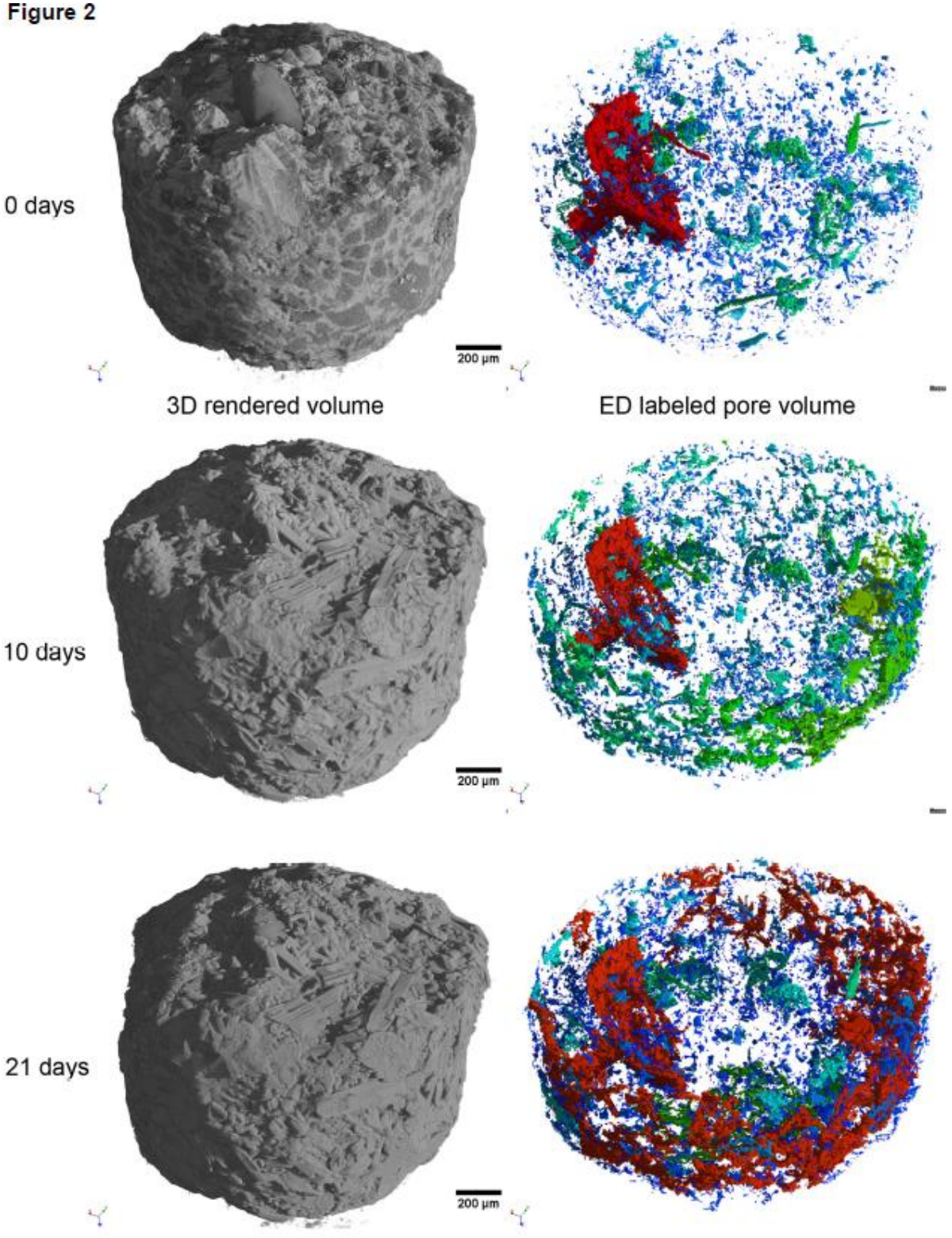

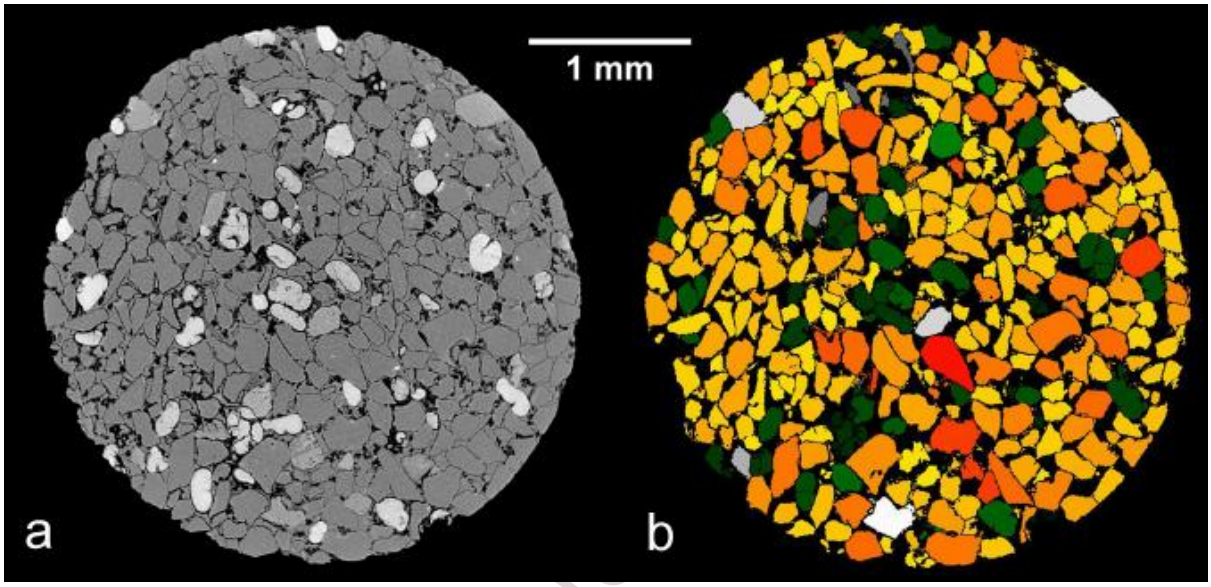

Figure 3

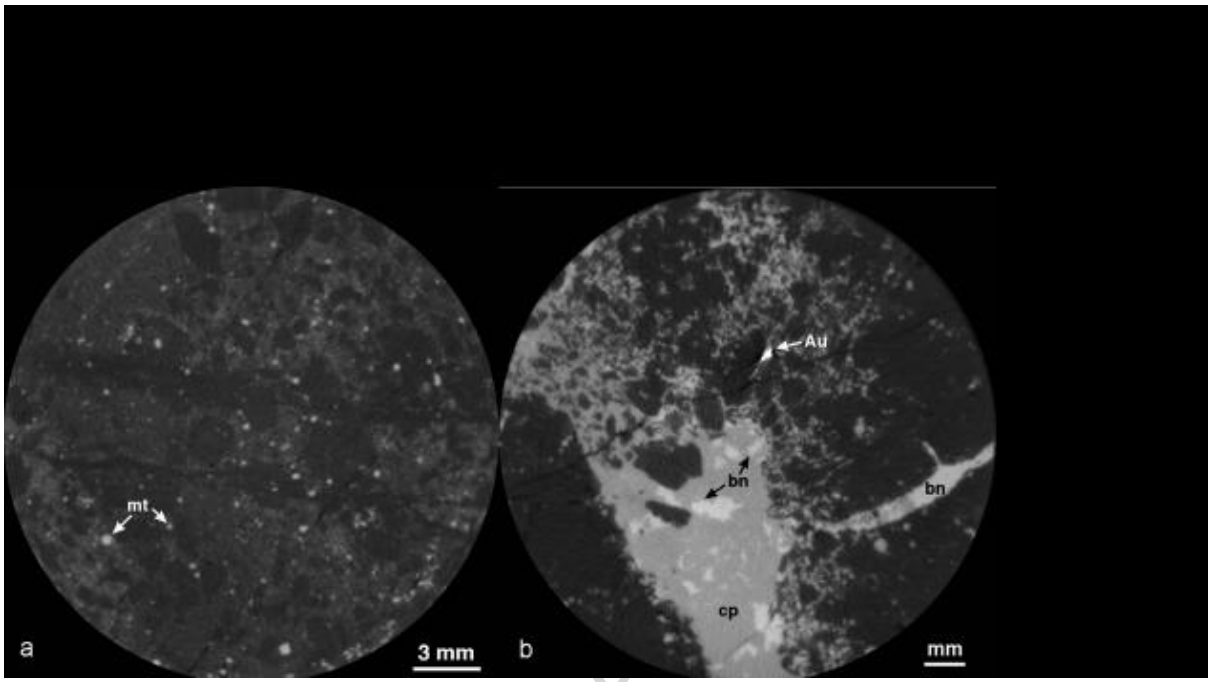

Figure 4

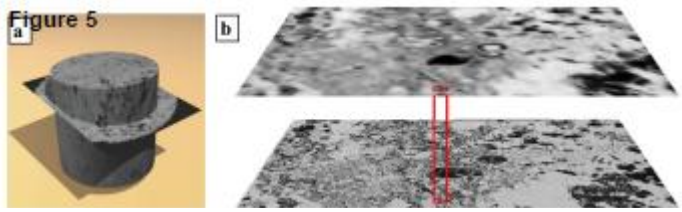

Figure 5

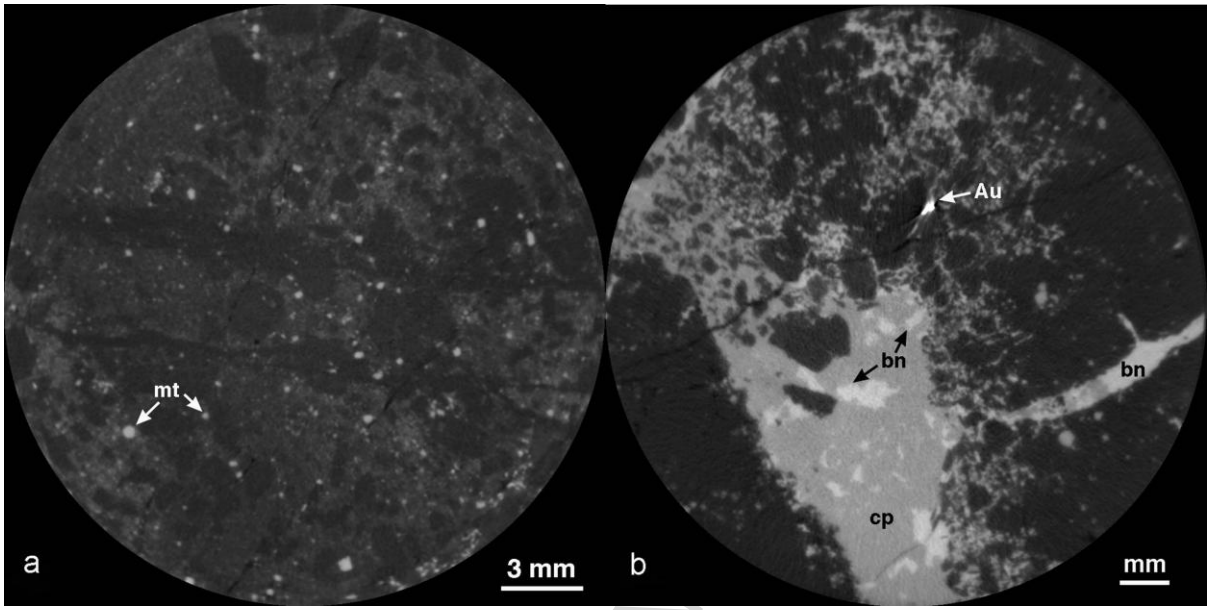

Figure 6

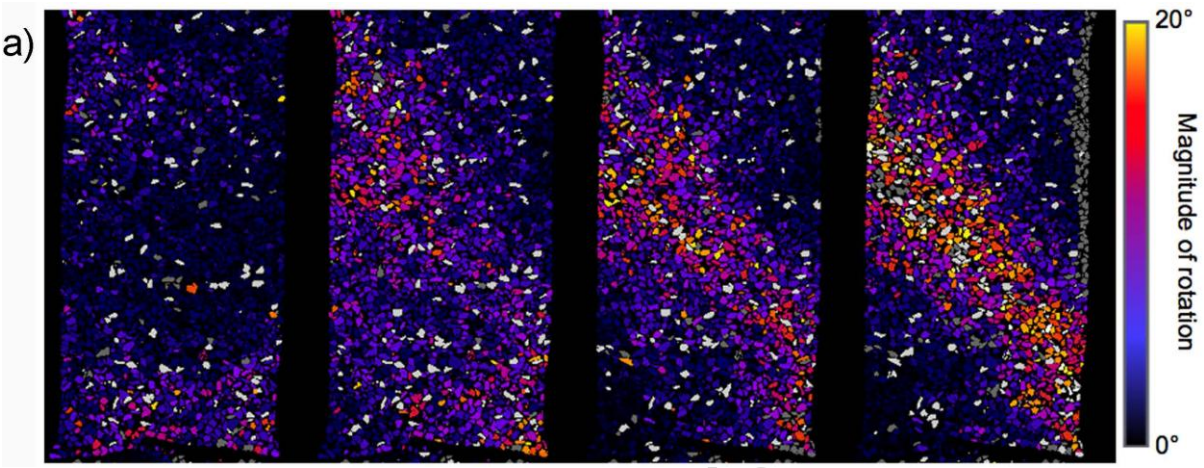

Figure 7a

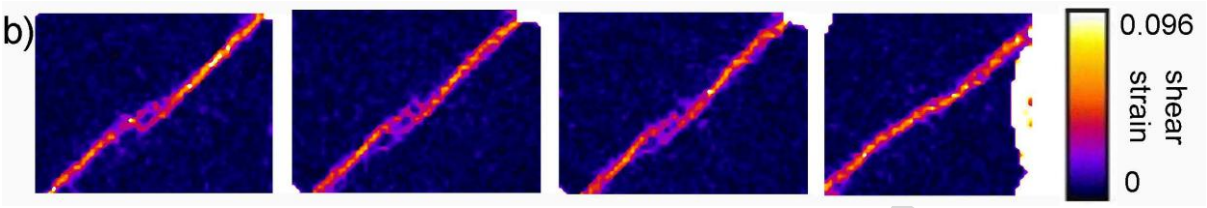

Figure 7b

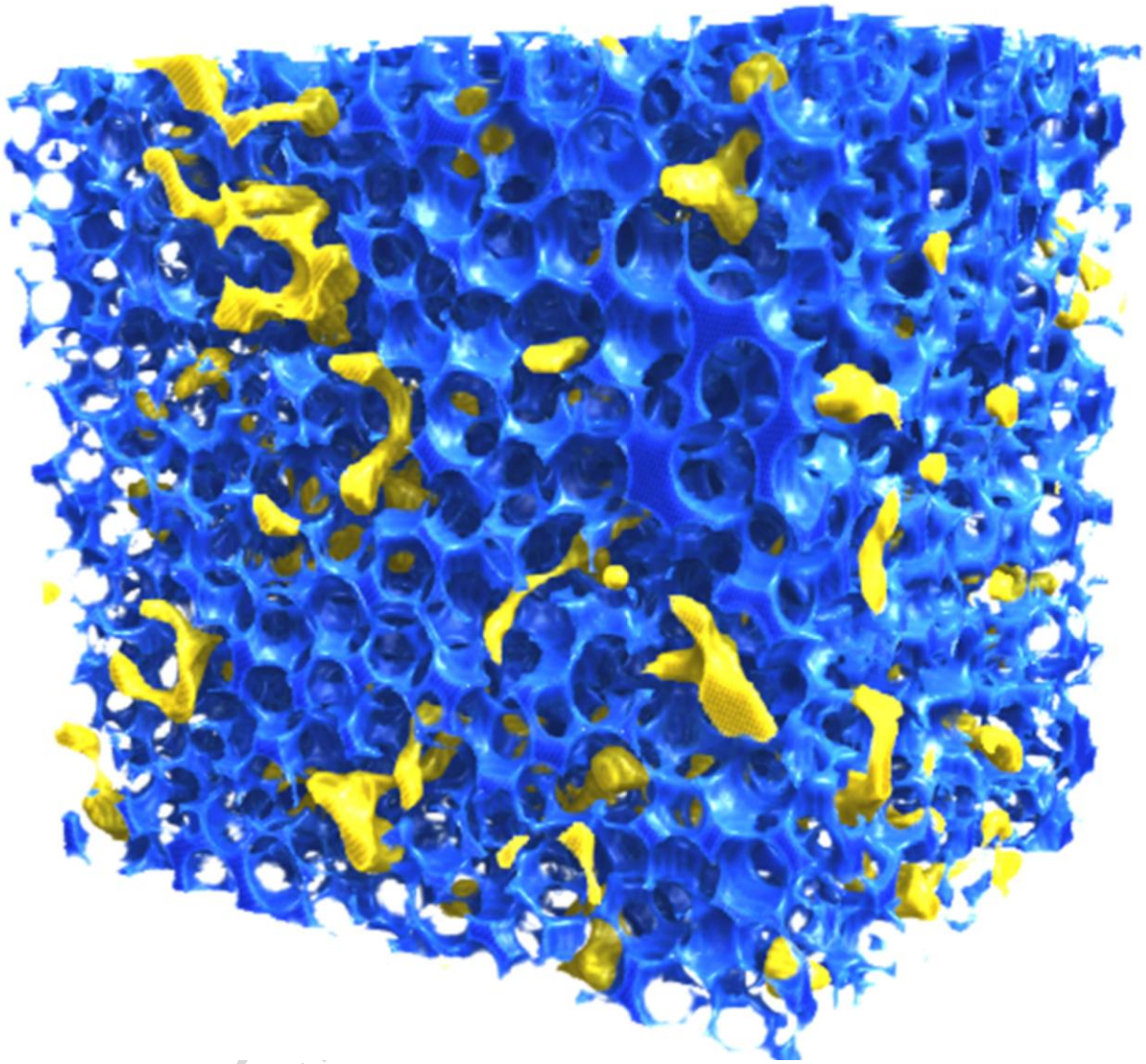

Figure 8

Figure 9